INVESTIGATING POLLUTANT TRANSPORT AND GENERATION IN URBAN LANDSCAPES

A Dissertation

Presented to the Faculty of the Graduate School

of Cornell University

In Partial Fulfillment of the Requirements for the Degree of

Doctor of Philosophy

by

Stephen Bernard Shaw

January 2009

INVESTIGATING POLLUTANT TRANSPORT AND GENERATION IN URBAN LANDSCAPES

Stephen Bernard Shaw, Ph. D.

Cornell University 2009

Suburban and exurban growth into formerly undeveloped areas frequently harm water quality. However, as planned landscapes, there is the possibility to implement measures within these suburban and exurban areas to mitigate deleterious changes to water bodies. To date, structural stormwater Best Management Practices (BMPs) such as detention ponds have demonstrated mixed potential to mitigate pollutant inputs over the long term, particularly in regards to dissolved nutrients. Additionally, such BMPs can be difficult to implement retroactively in mature, developed areas. Thus, a more fundamental understanding of sites of pollutant generation and transport pathways could lead to more refined and directed means of modifying landscapes to reduce pollutant loads to nearby surface waters. In particular, much as biogeochemical "hot spots" – areas of disproportionately high chemical and biological activity - have been surmised for natural systems, I propose analogous zones may be identified in more urban landscapes, defined by areas of small-scale landscape features that enhance pollutant generation and transport.

This dissertation will investigate spatially explicit processes that can be linked to small-scale spatial features in urban landscapes. The first chapter provides background on the current understanding of the relationship between small-scale spatial features and water quality. The second and third two chapters use a combination of theory and

experiments to develop a mechanistic particulate wash-off model, investigating the role of impervious surface roughness on rates of particulate loss. The fourth chapter examines catchments from a larger scale using weather radar. This chapter relates particulate wash-off to rainfall kinetic energy (a metric traditionally ignored in urban pollutant models) while questioning the use of antecedent dry days to explain the magnitude of wash-off (the routine explanation for variations in particulate loss). Overall, this body of work reassesses standard but frequently unvalidated assumptions used in estimating non-point pollutant loads.

BIOGRAPHICAL SKETCH

Stephen Shaw was born on June 13, 1978 in Kalamazoo, Mi. He earned his Bachelor of Science from Cornell University in 2000 and a Masters of Science from Cornell in 2005.

ACKNOWLEDGMENTS

I thank my wife Amanda for her continuous encouragement and support.

I thank my parents for their unconditional interest in my work.

I thank my faculty advisors – Dr. Todd Walter, Dr Jean-Yves Parlange, Dr. Jery Stedinger, and Dr. Tammo Steenhuis - for their guidance and helpful conversations.

I thank my brother for occasionally cyber-slacking to promptly answer my technical questions.

I thank my dog – Wallace – for exuberantly insisting on doing things not involving graduate school.

TABLE OF CONTENTS

LIST OF FIGURES

LIST OF TABLES

PREFACE

The work contained in this dissertation includes papers originally written for journal publication. As of October 2008, Chapter 2 had been published in Journal of Hydrology [Shaw, S.B., R. Mahklouf, M.T. Walter, J.-Y. Parlange. 2007. Experimental testing of a stochastic sediment transport model. Journal of Hydrology, 348(3-4): 425-430. (doi:10.1016/j.jhydrol.2007.10.014)]. Chapter 3 had been submitted for publication in Journal of Hydrology.

CHAPTER 1

INTRODUCTION - IMPROVING URBAN NON-POINT SOURCE MODELS BY DEVELOPING A BETTER UNDERSTANDING OF SMALL SCALE PROCESSES

Runoff from urban areas can transport pollutants such as nutrients, heavy metals, and pathogens to nearby water bodies (USEPA 1983). The urbanized landscape generating this pollutant laden runoff is typically described as a "non-point" pollutant source. In contrast to pollutants originating from a constant and obvious "point" source such as a factory, pollutants from non-point sources arrive intermittently in time and originate from diffuse locations across the landscape. Categorizing a pollutant source as being non-point inherently implies a lack of knowledge on where and when pollutant loads will occur. A central goal of water quality managers is to eliminate the need to describe a pollutant source as being non-point. This would then suggest they know where and when a pollutant originates and could mitigate its harmful impacts.

While this dissertation does not achieve the goal of transforming non-point sources to explainable point sources, it does provide new insights to improve models of non-point pollutant sources. A non-point source model is a quantitative tool to make the best prediction of where and when a given-sized pollutant load will occur. Most models of non-point source pollutants traditionally have been applied at a large spatial scale where watersheds thousands of hectares in size may be described by a single equation. In this introduction, I make the case that models of non-point source

pollutant loading can be improved by incorporating processes at the scale of meters to hundreds of meters, so-called small-scale processes.

In this chapter, I first describe the specific type of landscapes to which the work in this dissertation applies. Next, I provide an overview of the traditional, watershed- scale view of non-point source models. Then, I summarize recent work by other researchers considering small-scale descriptions of non-point source processes. Narrowing the focus further to the realm of the specific topics addressed in this dissertation, I review work on particulate wash-off from impervious surfaces. Finally, I outline the remaining chapters in the dissertation.

Mixed Land Surface Landscapes

This dissertation focuses on a specific type of urban land-use, landscapes with a mixture of land surface types. A typical example of such a landscape would be a suburban community where paved roadways adjoin managed turf grass interspersed with parcels of still undeveloped land. Kaye et al. (2006) note that such mixed land-use landscapes share characteristics of both highly urbanized and forested zones, making for potentially process-rich areas of study. A highly urbanized region may have large nutrient inputs but little biological activity and a highly engineered drainage system. However, more mixed land-use landscapes may still have large nutrient inputs, but they may also maintain a connection between engineered and natural processes, leading to complex pollutant transport and transformation dynamics. As a specific example, Wollheim et al. (2005) found that while mixed land-use landscapes may only have small remnants of previously natural zones, the fraction of retained nitrate inputs was nearly the same as in forested watersheds. This indicates a small region of intense biological activity overlapping with dominant transport

pathways in the mixed land-use watersheds. Recent research in urban National Science Foundation funded Long-Term Ecological Research (LTER) sites (Pickett et al. 2008) have corroborated this notion that mixed land-use landscapes may be as complex and deserving of research as more traditionally studied natural ecological systems.

Lumped Models

With the exception of recent work at LTER sites, water quality managers have treated pollutant transport in mixed-use landscapes as a relatively simple, applied engineering problem. From this applied-engineering perspective, these mixed land-use landscapes are primarily modeled as lumped systems in which a single representative set of parameters applies across the catchment. For example, in planning level models, annual pollutant loads are often estimated using land-use specific export coefficients (mass/unit area) multiplied by area (Schueler 1987). In some cases, loads are estimated by establishing a watershed event mean concentration (EMC) that can be multiplied by an estimated or measured runoff volume (Charbeneau and Barrett 1998, Lee and bang 2000, Chen and Adams 2007). Finally, in daily time step models such as the Storm Water Management Model (SWMM) (Tsihrintzis & Hamid 1998) pollutant loads are modeled using exponential build-up/wash-off functions calibrated with watershed-wide "effective" parameters.

In some cases, lumped models are calibrated against data collected in the watershed of interest. However, when an engineer is interested in making predictions in an unmonitored basin, the lumped approach has assumed that unmonitored watersheds can be related to monitored watersheds using readily observed characteristics, most typically land use. Numerous researchers have organized pollutant export factors or

EMCs by land use for use in models in unmonitored basins (see Reckhow et al. 1980, Clesceri et al. 1986, Line et al. 2002, Lin 2004). In most cases, the categories developed by land use planners (e.g. low-density residential, medium density residential) have been adopted as a proxy to describe differences in pollutant transport and generation processes among watersheds. Land-use has been used since the information is readily available and gross differences in land-use (such as between forested and agricultural) have proven effective at predicting differences in pollutant load (Jones et al. 2001). However, there remains a large amount of variability in estimated loads from within land-use categories. As an example in Table 1.1, measured annual phosphorus loads from seemingly similar "residential" areas range in value from 0.4 to 2.2 kg ha^{-1} yr^{-1}, discrediting the idea that a hydrologist can classify a landscape the same way a land use planner might.

Failing to discern differences in average load, lumped models have also guided conceptualization of the temporal dynamics of pollutant loss within storm events. Specifically, engineers have assumed the rate of mass loss is directly proportional to the amount of mass on the surface during a storm event, leading to the mathematically convenient assumption of exponential decay of pollutant mass with runoff quantity. However, actual examination of curves of cumulative mass loss during storm events rarely indicate that available mass becomes depleted and that mass loss slows later in a storm event (Lee and Bang 2000, Sansalone and Cristina 2004). Instead, cumulative mass loss frequently changes only in proportion to cumulative runoff.

Table 1.1 Selection of annual phosphorus export values associated with residential land use reported in the literature.

Source	Description	Phosphorus Load (kg/ha-yr)
Line et al. 2002 (Dodd et al. 1992)	Developed	1.06
Line et al. 2002 (Bales et al. 1999)	Residential	0.4
Line et al. 2002	Residential	2.3
Athayde et al. 1983	Residential	1.2
Reckhow et al. 1980 (Landon 1977)	High density with open grassed areas	0.56
Reckhow et al. 1980 (Kluesner & Lee 1974)	27% Impervious, Residential	1.1
Reckhow et al. 1980 (Much and Kemp 1978)	Residential	0.35
Reckhow et al. 1980 (Mattraw and Sherwood 1977)	Single Family Residential	0.21
Reckhow et al. 1980 (Betson 1978)	Suburban	0.43

Previous Work Examining Small-Scale Processes

To overcome discrepancies between theories of pollutant loss and actual observations of processes, there have been efforts to take a more sophisticated view of pollutant transport and generation in these mixed land-use landscapes. Chester and Gibbons (1996) observed that the fraction of impervious surface in a watershed could explain the degree of stream degradation, at least at a coarse level (say >20% impervious results in stream impairment). Hatt et al. (2004) found that connectivity of impervious surfaces to receiving waters had a stronger correlation to pollutant concentrations than imperviousness alone. Wishing to further acknowledge the role of position of the pollutant source, Sorrano et al. (1996) applied a transmission coefficient (to represent the proportion of phosphorus that travels between model cells without attenuation) in a raster model as well as accounted for runoff generation from each cell. Building on this work, Easton et al. (2007) constructed a nutrient export model on top of a spatially distributed hydrologic model operating at a 10 m spatial resolution for a watershed in upstate New York. As corroborated by runoff monitoring from specific subcatchment spatial features such as regions of managed lawn, unmanaged lawn, and scrub, Easton

et al. (2007) found that the load from spatial features was more dependent on runoff generating capacity and connection to outlet than the inherent surface type. Finally, Cadenasso et al. (2007) proposed a new means of land use classification using descriptors encompassing type of vegetation, type of surface in nonvegetated areas, and type of buildings. Their new classification system was better able to correlate annual nitrogen loads to watershed characteristics in comparison to traditional land classification methods.

These above mentioned studies clearly suggest that small-scale landscape features such as the type of surface, spatial position of the surface, and connectivity of the surface to receiving waters are critical to describing the degree and dynamics of pollutant loading in a given watershed.

Particulate Wash-off

The three remaining chapters of this dissertation address a specific niche in understanding small-scale processes: particulate wash-off from the impervious component of mixed-use landscapes. I focus on particulate matter since fine particulates can themselves be deleterious to water quality, but particulates also harbor nutrients, pathogens, and toxic chemicals (Sansalone and Buchberger 1997, Vaze and Chiew 2004).

Until recently, the understanding of particulate movement at a small-scale on impervious surfaces remained relatively rudimentary. For instance, Vaze and Chiew (2003) ran field experiments using two meter long concrete plots either covered with window screening or left uncovered. Rainfall was applied by an overhead sprinkler. The screened condition was intended to diminish the rainfall drop energy and

represent a treatment in which particle movement occurred only due to overland shear forces. After observing that the screened condition resulted in half as much mass loss as the unscreened condition, Vaze and Chiew (2002) concluded that rainfall and overland shear played approximately equal roles in particle initiation. But, experiments by Shaw et al. (2006) and Nino et al. (2003) clearly indicated that the roughness of the impervious surfaces inhibit the role of lateral shear force (a role in part overestimated by assuming shallow runoff behaves like the more well studied deep flow in stream channels), calling into question Vaze and Chiew's (2003) qualitative description of wash-off. Adopting soil erosion theory, Shaw et al. (2006) instead suggest that most particulate wash-off occurs as a saltation-like process in which rainfall ejects particles into the overland flow, and the particles laterally move a short distance in the overland flow before being captured on the surface to await ejection by another rain drop.

Dissertation Outline

The second and third chapters of this dissertation further develop the mechanistic wash-off model proposed by Shaw et al. (2006) by evaluating the physical basis of the model parameters and assessing the degree of particulate storage in elements of surface roughness. The fourth chapter considers particle storage on impervious surfaces at a larger spatial scale, using a time series of discharge and suspended solids concentration for an urban watershed to evaluate the build-up/wash-off models typically applied in urban areas. Additionally, the fourth chapter considers raindrop kinetic energy as a predictor of particulate load, an analysis that requires quantification of rainfall at a fine spatial and temporal scale. Overall, this work provides new insights into how small-scale processes may influence particulate pollutant generation and transport in mixed-use landscapes.

REFERENCES

Cadenasso, ML, STA Pickett, and K Schwarz. 2007. Spatial heterogeneity in urban ecosystems: reconceptualizing land cover and a framework for classification. *Frontiers in Ecology and Environment*, 5(2): 80-88.

Charboneau RJ, and ME Barrett. 1998. Evaluation of methods for estimating stormwater pollutant loads. *Water Environment Research*, 70(7): 1295-1302.

Chen, J. and B.J. Adams. 2007. A derived probability distribution approach to stormwater modeling. Advances in Water Resources, 30: 80-100.

Clesceri, N. L., Curran, S. J., and Sedlak, R. I. 1986. Nutrient loads to Wisconsin lakes: Part I. Nitrogen and phosphorus export coefficients, *Water Resources Bulletin* 22(6), 983-989.

Easton, Z.M., P. Gerard-Marchant, M. T. Walter, A.M. Petrovic, and T.S. Steenhuis. 2007. Identifying dissolved phosphorus source areas and predicting transport from an urban watershed using distributed hydrologic modeling. *Water Resources Research*, 43: W11414.

Hatt, B.E., T.D. Fletcher, and C.J. Walsh, and S.L. Taylor. 2004. The influence of urban density and drainage infrastructure on the connections and loads of pollutants in small streams. *Environmental Management*, 34(1): 112-124.

Jones, K.B., A.C. Neale, M.S. Nash, R.D. Van Remortel, J.D. Wickham, K.H. Ritters, and R.V. O'Neill. 2001. Predicting nutrient and sediment loadings to streams from landscape metrics: A multiple watershed study from the United States Mid-Atlantic Region. *Landscape Ecology*, 16(4): 301-312.

Kaye JP, Groffman PM, Grimm NB, L.A. Baker, and R.V. Pouyat. 2006. A distinct urban biogeochemistry? *Trends in Ecology and Evolution*, 21 (4): 192-199.

Lee, J.H., and K.W. Bang. 2000. Characterization of urban stormwater runoff, *Water Research*, 34(6): 1773-1780.

Lin, J. P. 2004. "Review of published export coefficient and event mean concentration (EMC) data," *WRAP Technical Notes Collection* (ERDC TN-WRAP-04-3), U.S. ArmyEngineer Research and Development Center, Vicksburg, MS. (website: www.wes.army.mil/el/wrap)

Line, D.E., N.M. White, D.L. Osmond, G.D. Jennings, and C.B. Mojonnier. 2002. Pollutant export from various land uses in the the upper Neuse River Basin. *Water Environment Research*, 74(1): 100-108.

Nino, Y., F. Lopez, and M. Garcia. 2003. Threshold for particle entrainment into suspension. *Sedimentology*, 50, 247-263.

Pickett, STA, ML Cadenasso, JM Grove, PM Groffman, LE Band, CG Boone, WR Burch, CSB Grimmond, J Hom, JC Jenkins, NL Law, CH Nilon, RV Pouyat, K Szlavecz, PS Warren, and MA Wilson. 2008. Beyond Urban Legends: An emerging framework of urban ecology, as illustrated by the Baltimore ecosystem study. Bioscience, 58(2): 139-150.

Reckhow, K.H., M.N. Beaulac, and J.T. Simpson. 1980. Modeling phosphorus loading and lake response under uncertainty: A manual and compilation of export coefficients. US EPA, Washington D.C., PB89-209001.

Sansalone, J.J. and S.G. Buchberger. 1997. Partitioning of first flush metals in urban roadway storm water. Journal of Environmental Engineering, 123: 134-143.

Sansalone, J.J. and C.M. Cristina. 2004. First flush concepts for suspended and dissolved solids in small impervious watersheds. Journal of Environmental Engineering, 130: 1301-1314.

Scheuler, T.R. 1987. Controlling Urban Runoff: A Practical Manual for Planning and Designing Urban BMPs. Metropolitan Washington Council of Governments.

Shaw, S.B., M.T. Walter, and T.S. Steenhuis. 2006. A physical model of particulate wash-off from rough impervious surfaces. *Journal of Hydrology*, 372: 618-626.

Sorrano, P.A., S.L. Huber, S.R. Carpenter, and R.C. Lathrop. 1996. Phosphorus loads to surface waters: A simple model to account for spatial pattern of land use. *Ecological Applications*, 6(3): 865-878.

Tsihrintzis, V. and R. Harmid. 1998. Runoff quality prediction from small urban catchments using SWMM. *Hydrological Processes*. 12:311-329.

U.S. Environmental Protection Agency (USEPA). 1983. Results of the Nationwide Urban Runoff Program: Volume I – final report, U.S. Environmental Protection Agency, PB84-185552, Washington, DC.

Wollheim WM, Pellerin BA, Vorosmarty CJ, et al. 2005. N retention in urbanizing headwater catchments. *Ecosystems*, 8 (8): 871-884.

Vaze, C. and F.H.S. Chiew. 2003. Study of Pollutant Washoff from Small Impervious Experimental Plots. Water Resources Research. V. 39(6): pp HWC 3-1 to 3-9.

Vaze, J., and F.H.S. Chiew. 2004. Nutrient loads associated with different sediment sizes in urban stormwater and surface pollutants. Journal of Environmental Engineering, 130: 391-396.

CHAPTER 2

EXPERIMENTAL TESTING OF A STOCHASTIC SEDIMENT TRANSPORT MODEL

2.1 Abstract

A stochastic model of sediment transport by rainfall-runoff was tested with a simple laboratory experiment. Although the conceptual basis of the model has been previously published (Lisle et al. 1998. *Journal of Hydrology*, 204: 217-230) and its mechanistic underpinnings were convincingly theorized, it had not been corroborated with measurements. Small-scale flume experiments, ~0.8 m long, with simulated rainfall were used to imitate "wash-off" of sediment (0.225 mm silica sand) from an impervious surface. Fitting two parameters (ejection and deposition rates) to minimize least squares error resulted in good agreement between stochastic model and measurements, R^2~0.9. However, the fitted parameter values differed from values that would be expected following Lisle et al's (1998) physical explanation of the ejection and deposition rates. While some of the discrepancy may be attributable to particle interactions, the conceptualization of deposition as a quiescent settling process in mechanistic erosion models may need to be reevaluated.

2.2 Introduction

We tested a stochastic sediment transport model (Lisle et al. 1998) against small-scale, laboratory observations of time dependent particle loss on a rough, impervious surface where particle ejection is primarily driven by rainfall, not overland shear. Most previous experiments of rainfall-driven, interrill erosion either only quantify steady-

state loss (Chaplot & Le Bissonnais 2000, Jayawardena & Bhuiyan 1999, Zartl et al. 2001) or involve many simultaneously occurring dynamic processes that make it difficult to isolate fundamental physical mechanisms (Profitt et al. 1991).

While capable of elucidating fundamental processes, the model is not without limitations; Lisle et al. (1998) note that their stochastic model is most useful to predict movement of particles present in a finite quantity with limited interactions with other particles or surrounding media. Experiments strictly on soils do not generally fulfill these conditions. However, an ideal scenario for testing the Lisle et al (1998) model is "wash-off" from an impervious surface with a finite supply of sediment. For this experimental condition, the critical assumption within the Lisle et al. (1998) model - that the probabilistic position of a single particle can represent the aggregate movement of multiple particles - is most likely attained.

Additionally, while an idealization of soil erosion, the Lisle et al. (1998) model may be directly applicable to modeling particulate transport processes in urban catchments. With the exception of Shaw et al.'s (2006) model that followed the deterministic approach of the Hairsine and Rose (1991) soil erosion model, previous wash-off models have primarily been empirical, were fitted only by calibration, and gave little insight into underlying physical wash-off processes (Akan 1988, Deletic 1997). This paper has two objectives: 1.) to test the model proposed by Lisle et al. (1998) against experimental wash-off data and 2.) to consider the physical basis of the model parameters.

2.3 Theory

Following Lisle et al. (1998), particle movement is assumed to be a Markov process with particles alternating between a state of rest or a state of motion, with the probability of being in one state or the other signified by *q* (at rest) and *p* (in motion). The spatial distribution of particles in motion or at rest across a one-dimensional surface is described by the "Kolmogorov-Feller" equations:

$$\frac{\partial p}{\partial t} + u\frac{\partial p}{\partial x} = -kp + hq \qquad (1a)$$

$$\frac{\partial q}{\partial t} = kp - hq \qquad (1b)$$

where *u* is the bulk flow velocity of the overland flow, *k* is a settling rate constant, and *h* is an ejection rate constant (Fig 2.1). For the initial conditions $p(x,0)=\delta(x)$ and $q(x,0)=0$, the system of equations 1a and 1b is solved as:

$$p_\delta(x,t) = H(\tau)H(\xi)\frac{h}{u}e^{-\xi}e^{-\tau}\sqrt{\frac{\xi}{\tau}}I_1\left[2\sqrt{(\xi\tau)}\right] + \frac{H(\xi)}{u}e^{-\xi}\delta(\tau) \qquad (2)$$

where $\xi = \frac{kx}{u}$, $\tau = h(t - \frac{x}{u})$, *H()* is the Heaviside step function, *δ()* is the Dirac delta function, and I_1 is a Modified Bessel function of the 1st order (Lisle et all 1998).

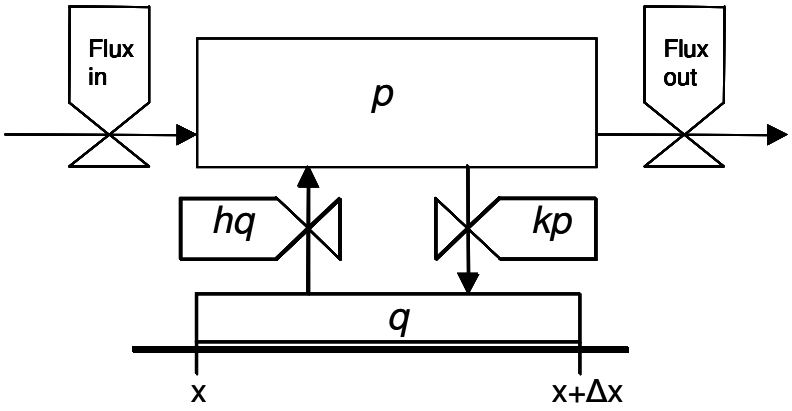

Figure 2.1. Schematic of rainfall driven particle movement in shallow flow described by Eqn.'s 1a and 1b. p is the probability of a particle being in motion while q is the probability a particle is at rest on the rough surface. k scales the rate of ejection of particles at rest while h scales the rate of deposition of particles in motion. Particles in motion move laterally with a velocity u.

For an initial condition of $p(L>\hat{x}>0,0) = C_0$, analogous to complete particle coverage of a surface length L, a convolution integral may be used:

$$p(x,t) = \int_{-\infty}^{\infty} p(\hat{x},0)\, p_{\delta}(x-\hat{x},t)\, d\hat{x} \tag{3}$$

As implied by the use of the convolution, we assume our experimental system will respond linearly due to the relatively low spatial density of particles on the flume surface (e.g. even with particle coverage of the entire flume surface, we assume there is not significantly greater interaction between particles than when we assume a pulse is applied).

The arrival time density (r) is given as

$$r(x,t) = up(x,t) \tag{4}$$

where this represents a rate of mass loss appropriate for plotting as a breakthrough curve at a fixed position of x.

Stochastically, the function $r(x=L,t)$ establishes the probability of a single particle being located at a position L at a time t. When considered in terms of the movement of many particles, $r(x=L,t)$ is the normalized particle loss at a position L at time t.

2.4 Methods

The experimental set-up and collection methods are only briefly summarized here and a fuller description is presented in Shaw et al. (2006). Rainfall and upslope flow were independently applied to an 80 cm long, 10.5 cm wide (width = W) stainless steel flume with a 4% slope (Fig. 2.2). A rough, flume bed was cut from a sheet of prismatic, polycarbonate diffuser used for recessed fluorescent light fixtures. A small Plexiglas stilling chamber with an overflow weir was used to control upslope flow. Three meters above the flume, rainfall was generated by four hypodermic needles that oscillated along two orthogonal tracks attached to the ceiling of the Soil and Water Lab at the Cornell University Department of Biological and Environmental Engineering. Using the flour pellet method (Laws and Parsons 1943), the average raindrop radius was 0.082 cm at a rainfall rate of 0.13 cm min^{-1}. An empirical relationship between flow and velocity was developed from five velocity measurements made over a range of overland flow rates applied only as upslope inflow. Flow velocity was determined by measuring the average time for a pulse of dye (FD&C red dye No. 40), injected into the flow stream with a pipette, to travel 40 cm; the measurement was made over the middle section of the flume to avoid end-effects. Velocities measurements were made in triplicate and the coefficient of variation was <~5%.

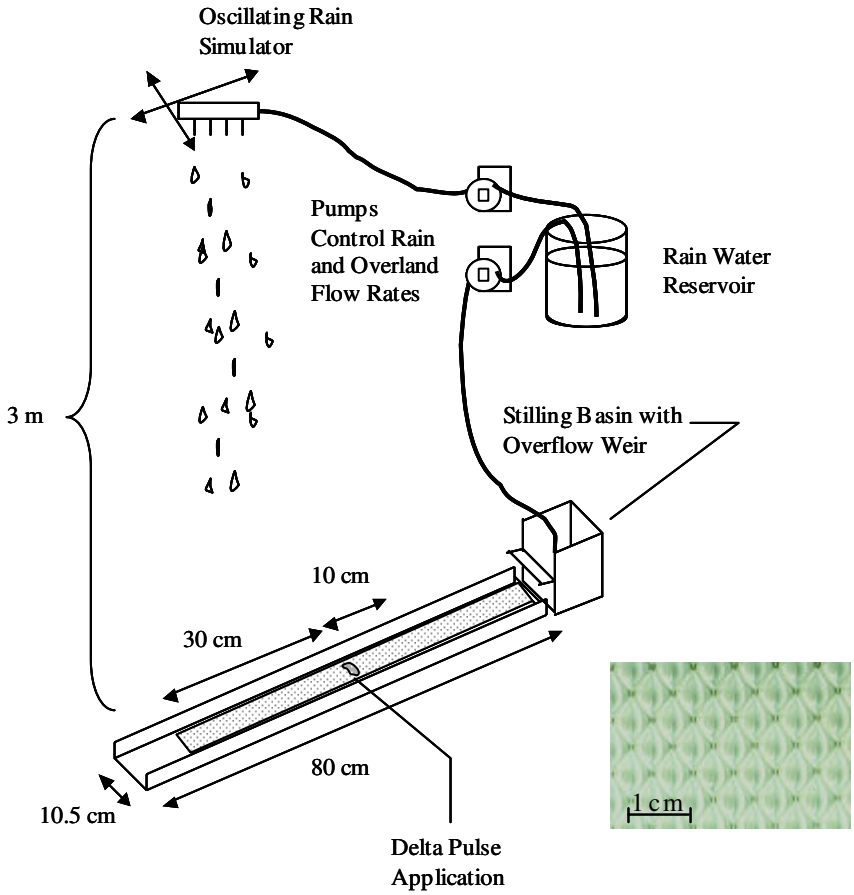

Figure 2.2. Schematic of experimental set-up and apparatus. Overland flow can be generated independently of rainfall by spilling water from the stilling basin. Inset is a scale image of the prismatic, polycarbonate diffuser plate used as the roughness surface in the experiments. Indentations are approximately 1 mm deep.

We applied 225 μm silica sand particles to the flume surface using two different initial conditions: a 2 cm band intended to represent a delta pulse (Runs 1 and 2) and complete coverage of 40 cm of the flume bed (Run 3). Particle spatial densities below 0.03 g cm^{-2} were used in order to minimize interactions between particles (Shaw et al. 2006). All runs were completed in duplicate. Flow off the end of the flume was funneled through a medium paper filter (Fisher Scientific). Each run was typically 10 minutes long and filters were changed every 45 seconds.

2.5 Results

The model (Eq. 4 and Eq. 2) was fit to the experimentally observed mass loss for a sediment pulse applied at the top of the flume (Runs 1 and 2 as shown in Figs. 2.3a, 2.3b). This scenario duplicates the conditions discussed in Lisle et al. (1998). In the model, the *x*-origin was taken at the center of the 2 cm pulse. "Fitting" entailed adjusting *h* and *k* in Eq. 2 to minimize the least squares error between simulated and observed (recall *u* was known from direct measurement). The model was also tested on conditions more closely approaching a real-world scenario in which particles completely cover a surface. The model (Eqs. 2-4) was fit to the wash-off from this initial condition (i.e. Run 3 as shown in Fig. 2.4), again minimizing least squares error between observed and simulated. The convolution (Eq. 3) was solved numerically with a spatial increment of 2 cm. We find that the Lisle et al. (1998) model can be used to suitably replicate the observed data in all cases (R^2>0.85). Of particular note, despite not including an explicit dispersion term, the stochastic model inherently results in a dispersed pulse. Table 2.1 summarizes the fitted *h* and *k* values as well as the R^2 values for each run. As would be expected, *h*, the "ejection rate," increases with increasing *P* while *k*, the "deposition rate," remains constant. Surprisingly though, for Run 3, *h* is not the same value as for Run 2 where the same *P* is used, possibly indicating that more interaction between particles occurs than we assumed or the model accounts for. We will address this point further in the Discussion.

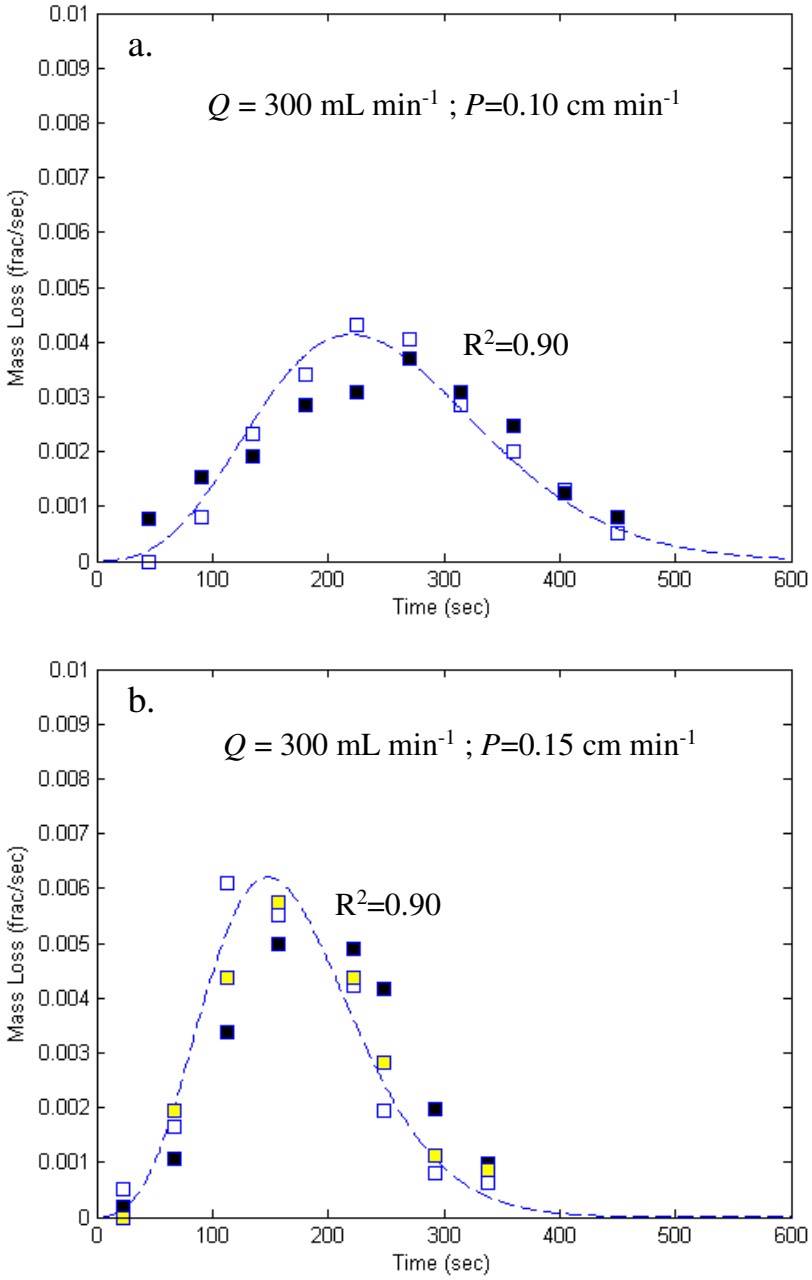

Figure 2.3. Lisle et al. (1998) model fit to experimental Run 1 (a) and Run 2 (b). Differing symbols indicate replicate trials. The dashed line indicates the model. The experimental runs used an initial 2 cm wide pulse of sand to replicate the delta function initial condition.

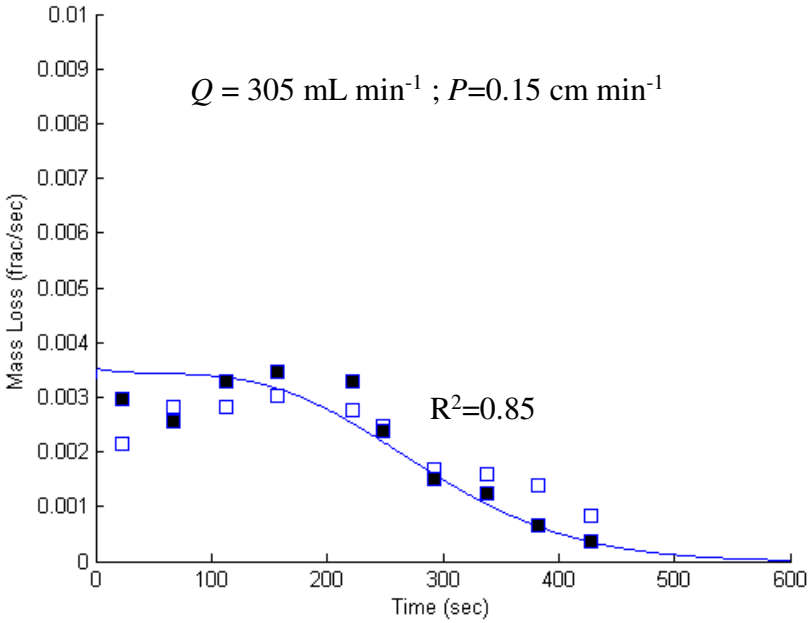

Figure 2.4. Model fit to experimental Run 3. Filled and open symbols indicate two duplicate trials. The solid line indicates the model. For this run, the surface initially was covered with sand grains from 0 to 0.4 m.

Table 2.1. Summary of model parameters for each run. Note, in Runs 1 and 2, particulate was applied in a 2 cm wide strip. In Run 3, particulate was applied over 40 cm of the flume surface.

Run	Q (mL/min)	P (cm/min)	initial M_0 (g cm^{-2})	u (cm sec^{-1})	h (sec^{-1})	k (sec^{-1})	R^2
1	300	0.10	0.03	8.3	0.050	3.2	0.90
2	300	0.15	0.03	8.6	0.070	3.2	0.90
3	305	0.15	0.02	8.6	0.050	3.2	0.85

As an illustration of model sensitivity to parameters, Figure 2.5 shows that when h is shifted above and below the best-fit value by 10%, the timing and magnitude of the peak also change by approximately 10%. Thus, any *a priori* estimate of h will require accurate estimation of underlying physical parameters, an issue to be discussed next.

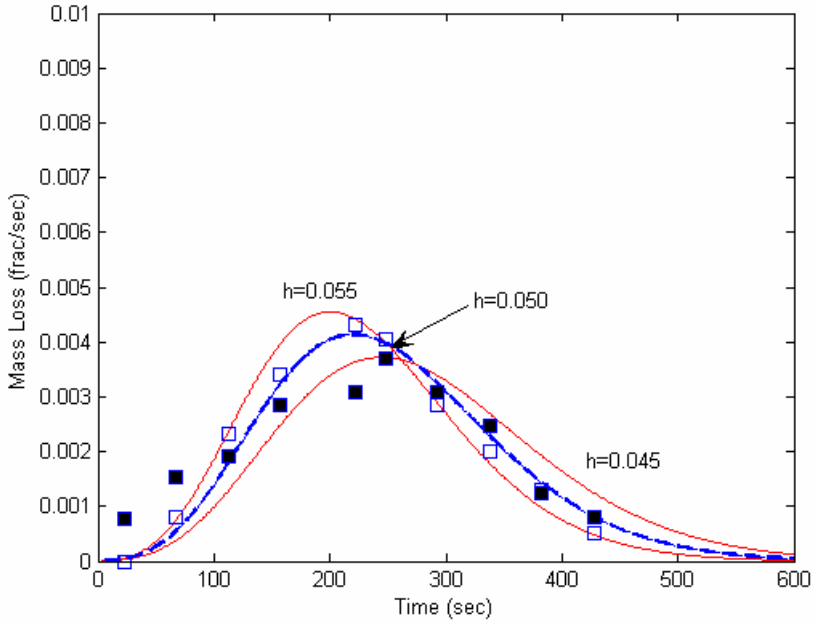

Figure 2.5. Sensitivity of Run 1 to a 10% change in *h*.

2.6 Discussion

Ideally, one would like to be able to select appropriate *h* and *k* values without model fitting. While stochastically, *h* and *k* parameterize the distribution of durations of rest and motion, respectively, Lisle et al. (1998) also attributed a physical meaning to *h* and *k*:

$$h = \frac{A_0}{V} P \tag{5}$$

$$k = \frac{v}{l} \tag{6}$$

where A_0 is the impact area of a rain drop (cm^2), V is the rain drop volume (cm^3) estimated from the measured drop radius assuming the drops are roughly spherical, P

is the rainfall rate (cm min^{-1}), v is the settling velocity (cm min^{-1}) and l is the flow depth (cm). Based on the formulation of Eq. 5 and Eq. 6, the magnitude of h reflects the fraction of surface area disturbed by rain drops per unit time, and the magnitude of k reflects the rate of time for a particle to settle over the flow depth, inherently implying a vertical settling process.

The accuracy of estimates of h and k from Eq. 5 and Eq. 6 is partially dependent on the estimates of the underlying physical quantities. Water depth (l) can be estimated using continuity ($Q / [u*W] = l$ where with Q = 5.36 mL/s (the average total flow for Run 1**,** 322 mL/min), u=8.3 cm/sec, and W=10.5 cm, l is 0.062 cm) . While this is the hydraulic flow depth (i.e. the depth of the flow profile that does not include the quiescent region within the roughness elements), a proper settling depth (l) would require subtraction of the particle diameter from the total depth. However, given the similar lengths of the roughness elements and the particles, the hydraulic flow depth was considered a reasonable proxy for the actual distance across which the particle would settle, i.e., $l \approx 0.062$ cm. An average settling velocity was determined experimentally (grains were hand-timed falling 40.0 cm in a 1 L graduated cylinder); based on the average of three replicates, $v \approx 170$ cm sec^{-1}.

But, unlike l and v, A_0 cannot be determined easily from either direct or indirect measurements, and a best estimates can only be drawn from highly controlled experiments on drop impact (Macklin and Metaxis 1975, Prosperetti and Oguz 1993) as well as inferences from experiments on aggregate mass loss from a flume (Shaw et al 2006). A simple way to generalize A_0 to experiments using various drop sizes is to consider the related quantity of the ratio between drop impact area radius and the drop radius. Previous investigators have suggested drop impact- to-drop radius values

ranging from approximately three (Macklin and Metaxas 1975) to seven (Prosperetti and Oguz 1993, Shaw et al. 2006).

Using the above estimates of the underlying physical quatities, h and k can be calculated as follows from Eq. 5 and Eq. 6. Assuming the drop impact -to- drop radius ratio needed to determine A_0 is approximately five (taking the mean of the available estimates) and using the 0.082 cm drop radius to calculate V, h should be ~0.39 sec^{-1} and ~0.59 sec^{-1} for P of 0.10 and 0.15 cm min^{-1}, respectively. Using Eq. 6 with l = 0.062 cm and v = 170 cm min^{-1}, k should be 46 sec^{-1}. Thus, we find that the model fitted parameters h and k (Table 1) are much smaller than the values that would be most expected given the physical interpretation of the parameters in Eq. 5 and 6.

To add some additional insight into the relationship between h and k, we note that Lisle et al. (1998) also related h and k to effective particle velocity, u_{eff}, and particle dispersion, D, for a long –time solution to Eqns. 1a and 1b:

$$u_{eff} = \frac{h}{h+k}u \tag{7}$$

$$D \sim \frac{hk}{(h+k)^3}u^2 \tag{8}$$

The long-time solution resembles the familiar advective-dispersion equation, thereby translating somewhat abstract h and k values into the more familiar quantities of dispersion and particle velocity. Any properly proportioned ratio of h and k can result in a reasonable u_{eff}, but including D constrains h and k for a given set of experimental conditions to one unique pair, a fact relevant to the following discussion.

The failure of Eq. 5 and Eq. 6 to suitably predict *h* and *k* values suggests at least two explanations, either A_0 and *v* are poorly estimated or the stochastic behavior of a single particle does not accurately represent the aggregate movement of many particles.. First, given that our estimate of A_0 is admittedly based on limited information, A_0 could reasonably be lower. But –in following the ratios established by Eq 7 and 8 – we would need to also decrease *v*, thus implying that deposition was not well modeled by a quiescent settling process. Given that particle movement during erosion is infrequently conceptualized as a series of step-like movements (Sander et al. 2007), there has been little motivation to make direct observations of the deposition process in very thin flows. In the few cases when deposition is included as a separate process in a model, settling rates are typically assumed to be known and ejection rates are used to fit the model (Shaw et al. 2006, Sander et al. 1996). Therefore, there is some possibility that deposition in thin flows has been consistently incorrectly modeled as a quiescent settling process when, in reality, it may be more of a capture process dependent on factors other than quiescent settling velocity. Supporting this notion, Parsons and Stromberg (1998) found experimentally a different power law relationship between particle diameter and travel distance different than would be expected assuming Eq. 6. Additionally, Nino et al. (2003), by direct visualization of particle movement in ~ 5 cm deep flow, did not even assume particle movement had occurred unless a particle traveled at least 100 particle diameters after ejection, a distance at least twice as long as would be expected given quiescent settling in their experiments. Thus, while evidence is limited, the deposition process may be much different than a simple settling process.

Alternatively, as a second possible reason Eq. 5 and Eq. 6 fail to predict suitable *h* and *k* values, , the model may be limited by the key assumption that the probabilistic

position of a single particle can represent the aggregate movement of multiple particles. Particle collisions could effectively decrease the settling rate by keeping a particle aloft longer (thus decreasing the *k* term) as well as decrease the effective drop impact area by damping impact energies and reducing particle ejection into the bulk flow (thus decreasing the *h* term). The settling rate and impact area could be adjusted to act as effective parameters -differing from the direct physical measurement of isolated phenomenon - or an explicit dispersion term could be added to Eq. 1a.

2.7 Conclusion

The stochastic erosion model by Lisle et al. (1998) was able to replicate experimental data when model parameter values were fitted. However, the model-fitted parameters did not agree with the physical interpretation of the parameters (Eq. 5 and Eq. 6), suggesting a need to account for particle interactions and, perhaps more importantly, to reassess the way in which deposition in thin flows is modeled.

REFERENCES

Akan, A.O. 1988. Pollutant Washoff by Overland Flow. *Journal of Environmental Engineering*, 113(4): 811-823.

Chaplot, V. and Y. Le Bissonnais. 2000. Field measurements of interrill erosion under different slopes and plot sizes. *Earth Surface Processes and Land Forms*, 25(2): 145-153.

Deletic, A., C. Maksimovic, and M. Ivetic. 1997. Modelling of Storm Wash-off of Suspended Solids from Impervious Surfaces. *Journal of Hydraulic Research*, 35(1): 99-117.

Hairsine, P.B. and C.W. Rose. 1991. Rainfall Detachment and Deposition: Sediment Transport in the Absence of Flow-Driven Processes. *Soil Science Society of America Journal*, 55: 320-324.

Jayawardena, A.W. and R.R. Bhuiyan. 1999. Evaluation of an interrill soil erosion model using laboratory catchment data. *Hydrological Processes*, 13(1): 89-100.

Laws, J. and D. Parsons. 1943. The Relation of Raindrop Size to Intensity. *Eos, Transactions of AGU*, 24: 452-460.

Lisle, I.G., C.W. Rose, W.L. Hogarth, P.B. Hairsine, G.C. Sanders, J.-Y. Parlange. 1998. Stochastic Sediment Transport in Soil Erosion. *Journal of Hydrology*, 204: 217-230.

Macklin, W.C. and G.J. Metaxas. *1976. Splashing of Drops on Liquid Layers.* Journal of Applied Physics 47(9): 3963-3970.

Nino, Y., F. Lopez, and M. Garcia. 2003. Threshold for particle entrainment into suspension. *Sedimentology*, 50, 247-263.

Parsons, A.J. and S.G.L. Stromberg. 1998. Experimental analysis of size and distance of travel of unconstrained particles in overland flow. *Water Resources Research*, 34:2377-2381.

Proffitt, A.P.B., Rose, C.W., and Hairsine, P.B., 1991, Rainfall Detachment and Deposition: Experiments with Low Slopes and Significant Water Depths, *Soil Science Society of America Journal*, 55:325-332.

Prosperitti, A. and H.N. Oguz. 1993. The Impact of Drops on Liquid Surfaces and the Underwater Noise of Rain. *Annual Reviews of Fluid Mechanics,* 25: 577.

Shaw, S.B., M.T. Walter, and T.S. Steenhuis. 2006. A physical model of particulate wash-off from rough impervious surfaces. *Journal of Hydrology*, 372: 618-626.

Sander, G.C., J.-Y. Parlange, D.A. Berry, M.B. Parlange, and W.L. Hogarth. 2007. Limitation of the transport capacity approach in sediment transport modeling, Water Resources Research, 43(2), W02403.

Zartl, A.S., A. Klik, and C. Huang. 2001. Soil detachment and transport processes from interrill and rill areas. *Physics and Chemistry of the Earth Part B – Hydrology, Oceans, and Atmosphere*, 26(1): 25-26.

CHAPTER 3

ACCOUNTING FOR SURFACE ROUGHNESS IN A PHYSICALLY-BASED URBAN WASH-OFF MODEL

3.1 Abstract

To date, urban wash-off models have largely ignored the role of surface roughness in controlling particulate mass loss. We propose a mechanistic model in which particles are ejected by raindrops from surface cavities and travel laterally at the velocity of the overland flow until they are recaptured. In the model, cavities of differing depth and diameter have different ejection rates. An analytical solution for a model consisting of two possible cavity geometries is fit to breakthrough curves from sediment wash-off experiments. The experiments are conducted on a 0.8-m flume under artificial rainfall with a surface constructed of casts of asphalt. The experiments use fine sand (~250 μm) and rainfall rates equivalent to that from a 2 year, 5-min. storm in non-coastal regions of the Northeastern United States. Model parameters can be attributed to specific physical features of the surface cavities, particles, or rainfall rate and can be determined with limited calibration. At the plot scale, with complete initial particulate coverage of the surface, the model replicates an initial first-flush and then settles to a more gradual loss rate which is noticeably different from the more rapid mass exhaustion implied by use of the common exponential wash-off model. Insights from this model could lead to improved design and placement of water quality management structures in urban landscapes.

3.2 Introduction

With a new focus on using localized management measures to control non-point source pollution in urban areas, further advances in our fundamental knowledge of spatially explicit pollutant generation and transport processes are needed (Potter 2006). In particular, estimating wash-off of particulate matter still frequently relies on a lumped, catchment scale exponential model or variants (Alley 1981, Tsihrintzis and Hamid 1998, Chen and Adams 2007). While a few spatially distributed models have been developed (Akan 1988, Deletic et al. 1997), they have a limited physical basis and make no observation of the small-scale, internal catchment processes. Conversely, of the few published plot scale experiments (Sansalone 1998, Vaze and Chiew 2003), most have little quantitative analysis. As an exception, Shaw et al. (2006) used experiments to evaluate a simple rainfall driven transport model for cases in which shear flow has a negligible role in particle entrainment. However, the experiments were conducted on a uniformly rough surface unlikely to represent the trapping processes associated with the irregular cavity geometries on actual urban surfaces such as asphalt (Deng et al. 2005, Nino et al 2005).

In this paper, we 1.) propose a mechanistic wash-off model that accounts for trapping within surface roughness elements, 2.) compare the model to experimental results (indoor, 80 cm flume) 3.) evaluate means to parameterize the model *a priori* based on physical features of the surface, and 4.) explore the suitability of the model when applied to a larger 20 m reach scale.

3.3 Theory

Similar to Shaw et al. (2006), we assume that particle movement occurs by a sequence of jumps in which particles are either at rest on the rough surface or in motion

suspended in shallow overland flow (Figure 3.1). Movement is initiated only by raindrops, not by overland shear flow, due to surface cavities. Our own observations agree with experiments by Nino et al. (2003) which found that rough surfaces shift the threshold for incipient motion upwards, increasing the range of flow conditions in which raindrop initiated movement dominates. We assume particles on the bed surface can fall into multiple cavity geometries or "bins", each with a different rate of ejection. Thus, the formulation is akin to a simple multiple rate mass transfer (MRMT) model (e.g. Pedit & Miller 1994, Haggerty and Gorelick 1995, Wang et al. 2005) or a two site transport model in which both sites proceed kinetically (Van Genuchten & Wagenet 1989), approaches more traditionally applied to solute transport in groundwater. Each bin is considered to occupy a fraction of the surface (*f*) characterized by cavities of similar diameter and depth that control ejection at a given rate. Particles enter the shallow flow by raindrop-induced ejection at multiple rates, corresponding to *i* different bins, and settle-out of the shallow flow at a single rate. While settling-out, suspended particles are advected in the overland flow at the same velocity as the flow.

Following Hairsine and Rose (1991) for the case in which overland flow does not exceed the threshold for particle entrainment, mass conservation of suspended particles in the water layer is given by:

$$\frac{\partial M_s}{\partial t} + \frac{\partial v M_s}{\partial x} = \sum_{i=1} h_i M_i - k M_s \qquad (1)$$

where M_s is the suspended particle mass (g), x is the downslope distance, and v is the overland flow velocity (cm s^{-1}), h_i is the ejection rate constant (s^{-1}), M_i is the immobile material in bin i (g), and k is the capture rate constant (s^{-1}).

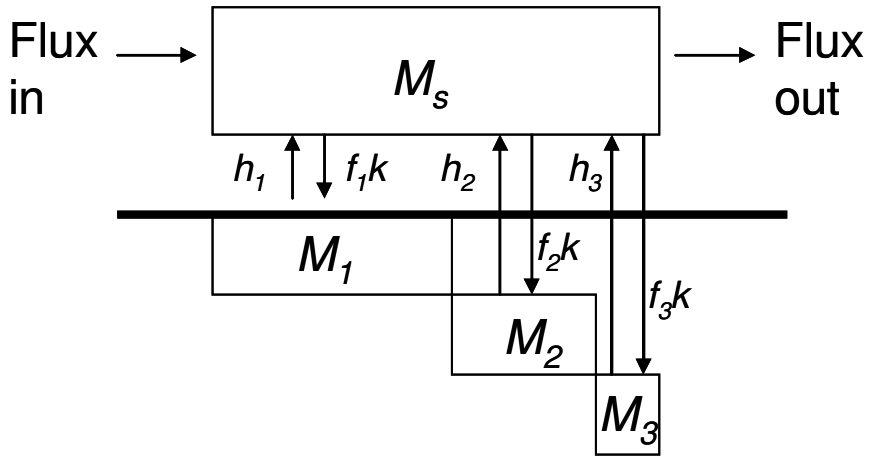

Figure 3.1. Schematic of mass exchange in a multi-trap system. In this case there are three bins - M_i, each covering a different fraction, f_i, of the total surface and with a different ejection rate, h_i. k is the settling rate from the suspended mass pool, M_s. Only particles in M_s can move laterally.

Particle mass on the surface in different bins at a distinct spatial position is given by:

$$\frac{\partial M_i}{\partial t} = f_i k M_s - h_i M_i \qquad (2)$$

where f_i is the fraction of particles captured by bin i, which we assume to be related to the i^{th} distinct cavity size on the surface. Note, $\sum_{i=1} f_i = 1$. Herein, we will refer to Eqn.'s 1 and 2 as the multirate mass transfer model (MRMT).

Following Lisle et al.'s (1998) development of a stochastic particulate transport model, the ejection rate constant is assumed to be given by:

$$h_i = \frac{A_i}{V} P \qquad (3)$$

where A_i is the area influenced by the drop impact, V is the drop volume, and P is the precipitation rate (cm min^{-1}). On a flat surface with a shallow water depth, A_i is dictated by the drop energy and particle size (Mihara 1952, Macklin & Metaxis 1976). However, we hypothesize that a rough surface will compartmentalize drop impacts

and constrain A_i. Therefore, the fraction of the surface with smaller diameter and deeper cavities will have a lower h.

Finally, the capture rate constant (k) proposed by Lisle et al. (1998) assumed a quiescent settling process ($k = v_{set} / d$) where v_{set} is the particle settling velocity and d is the average depth of the advecting flow layer (cm). However, more recent work suggests capture may not be due to settling alone and k may represent an effective settling rate (Shaw et al. 2007).

3.4 Methods

Using a small flume situated under an artificial rain machine, we observed the rate of wash-off of particulate "pulses" from two different surfaces under the same upslope flow and rainfall rates.

Characterization of Roughness Surface

Molds of parking lot pavement were made from two sites near Riley-Robb Hall, Cornell University, Ithaca, NY using silicone mold making rubber (Dow Corning HS II). The sites were selected to have different surface roughness characteristics, one lot being newly installed. From both sites, five 10 cm long, 1 mm wide strips were trimmed from each mold and the cross-sectional profile digitally imaged using a high-resolution scanner (Umax Astra 4000U) (example shown in Figure 3.2). For each strip, the width of all crevices was measured at successively deeper 0.5 mm increments.

Experimental Runs

Laboratory methods closely followed the set-up and approach used in Shaw et al. (2006, 2007). An 80 cm long, 10.5 cm wide stainless steel flume with a 4% slope was located beneath a computer-controlled rainmaker generating ~0.08 cm radius drops. Overland flow was directly applied through a small Plexiglas stilling chamber at the upslope end of the flume. A primary difference from Shaw et al. (2006) was the use of smaller particles (225 μm) closer in size to the median observed in wash-off (100 μm, Sansalone et al. 1998) as well as higher upslope overland flow rates (~10 l min^{-1} m^{-1}) equivalent to 0.24 cm min^{-1} rainfall accumulated at the end of an impervious 40 m reach. The rainfall rate was 0.24 cm min^{-1}, equivalent to the intensity of a 2 year, 5 minute storm in the non-coastal regions of the Northeastern United States (NOAA 1977).

The flume surface consisted of a plaster-of-paris cast of a 20 cm by 10 cm silicone rubber mold made during the roughness characterization. Runs were carried out on the two different surfaces (herein referred to as Lot 1 and Lot 2) described in the roughness characterization (Figures 3.2a and 3.2b). For each surface, three identical casts of ~20 cm were adjoined to cover a 60 cm length of the flume. The plaster-of-paris was spray coated with a latex paint in order to minimize water seepage into the cast.

We applied 10 g of 225 μm quartz sand particles in a 10 cm long strip within the interval 30 to 40 cm from the bottom of the flume. Flow off the end of the flume spilled into a stainless steel trough that diverted the sediment-laden water into a funnel fitted with a 100 μm metal screen. Collection funnels were changed approximately

every 45 seconds. Recovery averaged 90% with any losses assumed to occur uniformly throughout the run. Parameters for each run are summarized in Table 3.1.

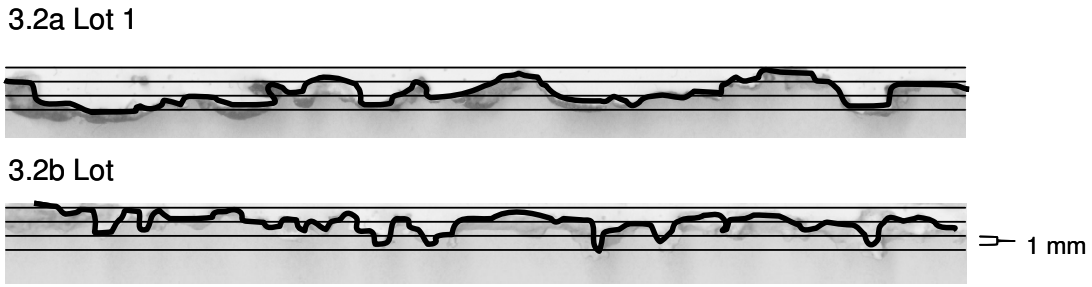

Figure 3.2a and 3.2b. Profiles of asphalt surfaces from two different parking lots. The mold is shown inverted, as applied to the pavement. The negative space – gray color – would be the pavement with it's surface traced by the bold line. The image is enlarged 2x.

Table 3.1. Summary of roughness surface experiments. Values in brackets indicate standard errors.

Run	q (mL min^{-1} m^{-1})	P (cm min^{-1})	*Length (cm)*	h_1 (sec^{-1})	h_2 (sec^{-1})	h_3 (sec^{-1})	f_1	f_2	f_3	k (sec^{-1})
Lot 1	10200	0.24	35	0.063 (0.017)	0.005 (0.007)	---	0.98 (0.025)	0.02	---	10 (2.01)
Lot 2	10400	0.24	35	0.045 (0.0015)	0.003 (0.0006)	---	0.96 (0.011)	0.04	---	10 (1.75)
Plot Scale	100	0.03	2000	0.075	0.01	0.001	0.70	0.15	0.10	0.056

Model Implementation

An analytical solution for the M_s loss rate for a two bin MRMT (i=2) with initial conditions $M_s(x,0) = \delta(x)$ and $M_1(x,0) = M_2(x,0) = 0$, was found via Laplace Transforms of Eqn.'s 1 and 2. The solution consists of three terms (as ordered below in Eqn. 4): a convolution in which movement through the bin 2 cavities acts as the response function for movement through the bin 1 cavities, movement through bin 1 cavities alone, and movement through bin 2 cavities alone:

$$M_s(x,t) =$$

$$H(\xi)\hat{h}_1\hat{h}_2 e^{-\xi}\int_0^t H(\tau_1)H(\tau_2)\exp(-\tau_1-\tau_2)\sqrt{\frac{\xi f_1\hat{h}_1}{\tau_1}}\sqrt{\frac{\xi f_2\hat{h}_2}{\tau_2}}I_1\left[2\sqrt{\xi\hat{h}_1 f_1\tau_1}\right]I_1\left[2\sqrt{\xi\hat{h}_2 f_2\tau_2}\right]dt' +$$

$$+H(\tau_1)H(\xi)\hat{h}_1 e^{-\xi-h_1\tau}\sqrt{\frac{\xi f_1}{\hat{h}_1\tau_1}}I_1\left[2\sqrt{f_1\hat{h}_1\xi\tau_1}\right]+\frac{H(\xi)}{u}e^{-\xi}\delta(\tau_1)+$$

$$+H(\tau_1)H(\xi)\hat{h}_2 e^{-\xi-h_2\tau}\sqrt{\frac{\xi f_2}{\hat{h}_2\tau_1}}I_1\left[2\sqrt{f_2\hat{h}_2\xi\tau_1}\right] \qquad (4)$$

where $\tau_1 = t' - \frac{x}{u}$, $\tau_2 = t - t' - \frac{x}{u}$, $\xi = \frac{kx}{u}$, $H()$ is the Heaviside Step function, I_1 is the Bessel Function of the first order, and $\delta()$ is the Delta Dirac function. The convolution within Eqn. 4 is evaluated discretely using a time step of 10 sec.

For the model, overland flow velocity was estimated using Manning's Equation with a Manning's roughness of n=0.03 (Anderson et al. 1998), also similar to the 0.025 value used by Christina and Sansalone (2002) for pavement. Direct measurement of velocities on the laboratory flume indicated that Manning's Equation was within 10% of the observed v. Experimental flow velocity was determined by measuring the time for dye (FD&C red dye No. 40), injected into the flow stream with a pipette, to travel a set distance.

Settling depth, d, was determined by continuity. d's were large enough that terminal velocity was reached. Settling velocity was determined experimentally (grains were hand-timed falling 40 cm in a 1 L graduated cylinder): we found v_{set} = 170 cm min^{-1}.

3.5 Results & Discussion

Modeling the Breakthrough Curves

Assessing the experimentally observed breakthrough curves (Figure 3.3a & 3.3b), peak loss on Lot 2 is slightly delayed in comparison to Lot 1. Additionally and more

significantly, the Lot 2 surface exhibits a greater amount of tailing than Lot 1 with traces of particulate detected after 2000 s. while none is detected after 1000 s. on Lot 1. In terms of the breakthrough time of the center of mass of the pulse, 50% of the applied mass is lost after ~335 s on the Lot 1 surface and 50% is lost after 550 s on the Lot 2 surface. These differences in wash-off behavior correspond to obvious visual differences in the roughness of the two surfaces; the Lot 1 surface has fewer narrow, Figure 3.3a. deep crevices and many more shallow broad crevices in comparison to Lot 2 (Figure 3.2).

The breakthrough curves from both surfaces were reasonably fit (R^2~0.96 for Lot 1 and R^2~0.98 for Lot 2) using the solution to the 2 -bin MRMT model, Eqn. 4 (Figure 3.3). Parameters were manually adjusted to maximize the R^2 value. However, a two bin model requires four parameters (f_1, h_1, h_2, and k), and multiple parameter combinations can produce a similar fit. As in many cases where a model displays equifinality, certain parameter choices are more physically suitable. While not merely calibration parameters, we will demonstrate an underlying physical basis for each of the four parameters and suggest means to identify model parameters *a priori* in future cases.

Figure 3.3a

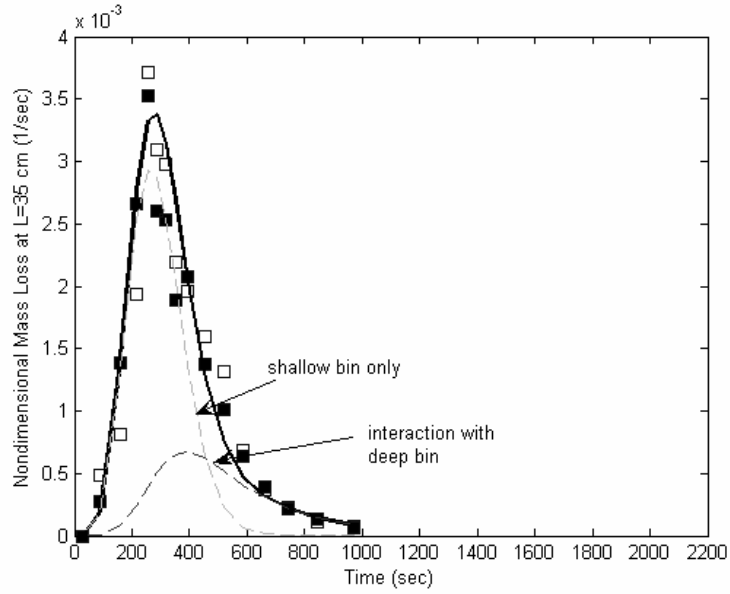

Figure 3.3b.

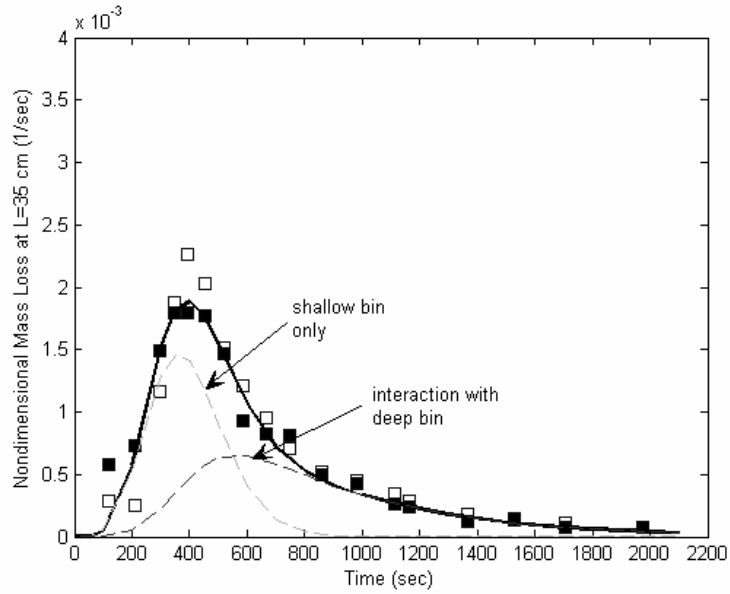

Figures 3.3a and 3.3b. Model simulations fit to breakthrough curves for 225 µm particulate movement on 60 cm asphalt casts from Lot 1 (3a) and Lot 2 (3b). Symbols indicate observed values (filled and unfilled are replicates); solid line is the model. For both runs, upslope flow (q) and rainfall (P) were nearly the same, ~10,300 ml min^{-1} m^{-1} and 0.24 cm min^{-1} respectively. Model parameters are summarized in Table 3.1. The R^2's for the model runs in 3.3a and 3.3b are 0.96 and 0.98, respectively. The dashed lines illustrate the contribution to mass loss from different model components.

Comparison to the Fokker-Planck Equation

As a starting point for evaluating the model parameters, we apply the Fokker-Planck equation with $M(x,0) = M_0\delta(t)$ (Fischer et al. 1979, Eqn 2.28). Note, since we are fitting a breakthrough curve, the standard Fokker-Planck solution is multiplied by u_{eff} so as to calculate mass flux and not concentration (see Lisle et al. 1998, Eqn 12). As a traditional approach to fitting breakthrough curves, the Fokker-Planck equation provides a point of comparison to the two-bin model as well as a means to estimate parameters of aggregate movement, effective velocity (u_{eff}) and dispersion (D).

To fit the Fokker-Planck equation, an experimental u_{eff} can obviously be determined from the observed breakthrough curve by taking the quotient of the travel distance, L, and the time to peak. An experimental D can be determined from the observed breakthrough curves by manipulating the solution to the Fokker-Planck equation with a delta pulse boundary condition so when $t=L/u_{eff}$:

$$D = \frac{u_{eff}^2}{4\pi M_{\max}^2 t} \qquad (5)$$

By this approach, the Lot 2 breakthrough is fit with u_{eff}=0.0778 cm s^{-1} and D =0.33 cm^2 s^{-1}.While capturing the timing and magnitude of the peak, the width of the peak is slightly exaggerated and, the degree of tailing is underestimated (Figure 2.4). We will see below how a fundamentally different model structure is needed to fit these seemingly minor discrepancies.

The h and k parameters in a MRMT can be related to D and u_{eff} in the Fokker Planck equation. But, only at long times is the Fokker-Planck equation identical to the MRMT model. With the Fokker Planck equation and the 2-bin model in Laplace space (see Appendix), we performed a Taylor Series expansion on terms within the

exponential functions. Excising all terms above 2nd order, we found the Fokker Planck and MRMT formulations were identical. However, since our experiment does not take place at a scale appropriate for a long-time approximation, we can use the Fokker-Planck equation to inform our choice of h and k, but we would not expect an identical fit to the observed breakthrough. But, by relating to D and u_{eff}, we gain some insight into how h and k interact to result in aggregate particle behavior.

For a two bin model, we find (see appendix for derivation):

$$u_{eff} = \frac{uh_1h_2}{(h_1h_2 + kf_1h_2 + kf_2h_1)} \tag{6}$$

And

$$D = \frac{u^2\left(\frac{f_1k}{h_1^2} + \frac{f_2k}{h_2^2}\right)}{\left(1 + \frac{kf_1}{h_1} + \frac{kf_2}{h_2}\right)^3} \tag{7}$$

Eqn.'s 6 and 7 will be of some use in constraining h and k as discussed below.

Selecting f_1

Since f_2=1-f_1, we can modify Eqn. 6 and 7 to show that u_{eff} and D are relatively insensitive to f_1 as long as we know f_1 is near 1. f_1 mainly controls the magnitude of the peak and the magnitude in the transition to the tail, features not captured by u_{eff} and D. The reason for this behavior can be seen in Figure 3.3 (dashed lines) where the contribution of the individual terms in the model solution (Eqn. 4) are shown. Adjusting f_1 shifts the emphasis on each of these two peaks.

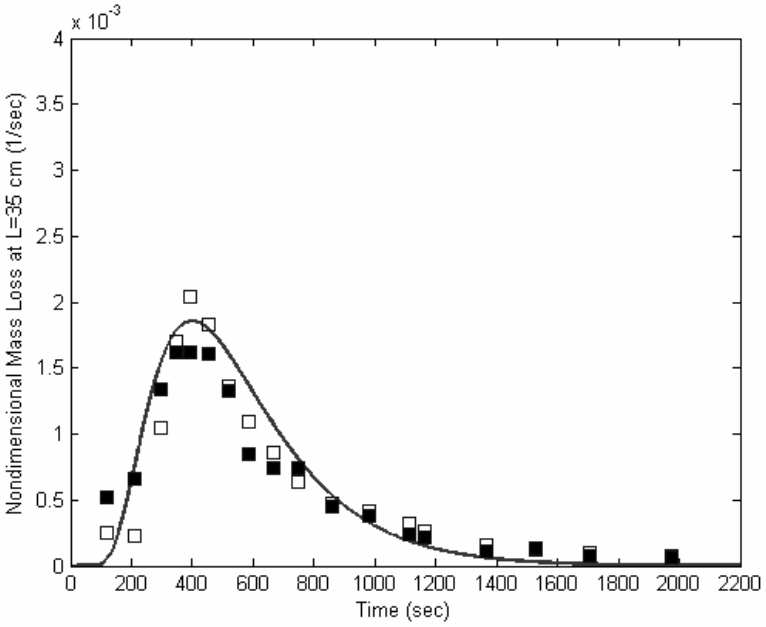

Figure 3.4. Fokker-Planck equation fit (solid line) to Run 2 observed (symbols). D (0.33) and u_{eff} (0.0778) in the Fokker-Planck equation were determined from inspection of the breakthrough data (see Eqn.5).

If there is little tailing, f_1 is large (~1), the first peak dominates, and the overall breakthrough resembles the first component. If f_1 is smaller (i.e. f_1=0.90, not shown), most particles fall into deep crevices, the second peak dominates such that the overall breakthrough resembles the second component. Distinct features of our observed breakthrough curves arise from overlap between the two components; namely, the asymmetrical, high "shoulder" of the receding breakthrough curve can only be duplicated with the overlap of the rising second component with the falling first component.

To some degree, f_1 can be estimated from the physical characteristics of the rough surfaces. We hypothesize that the distinction between a deep and shallow crevice depends on an interaction between average cavity depth and width. From the surface characterization, we can determine the fraction of each surface covered by cavities of

a certain depth to width ratio. Evaluating several possible ratios involving the deeper crevices (the deepest was ~2.5 mm), we found Lot 1 and Lot 2 consisted of 3.5% and 5.5%, respectively, of crevices greater than 2 mm deep and less than 8 mm wide. And considering another depth-to-width ratio, we found Lot 1 and Lot 2 consist of 1.4% and 2.7%, respectively, of crevices greater than 2mm deep and less than 4 mm wide. This range of depth to width ratios seems to envelope our calibrated f_1 values of 2% and 4% for Lot 1 and Lot 2, respectively.

Finally, since f_1 is relatively independent of u_{eff} and D, f_1 is also relatively independent of h_i and k. With k constant, one would not be able to compensate for changes in f_1 with changes in h. But, with f_1 constant, h and k can be used to compensate for one another.

Balancing k and h_i's

With an f_1 selected as discussed above, one must then narrow the range of h and k. h and k will be linked by Eqn.'s 6 and 7 – a large h must be accompanied by a large k. If we can establish the range of either h or k, we constrain the other. k relates to the particle capture rate and should be partially dependent on the particle size (in terms of settling velocity) but also potentially on surface characteristics. Recent work suggests that particle capture is not necessarily well modeled as a quiescent settling process (Parsons & Stromberg 1998, Nino et al. 2003, Shaw et al. 2007), a simplification traditionally assumed in mechanistic erosion models. If the particle capture were solely due to quiescent settling, with a v_{set} of 2.83 cm s^{-1} (determined experimentally by hand timing the fall of the particles over 40 cm) and an average d=0.1 cm, k=28.3 s^{-1}. On a uniformly rough surface consisting of shallow, oblong depressions (not necessarily efficient at trapping), using the same sized particles, Shaw et al. (2007)

found k=3.8 s^{-1} from modeling. We consider these values to be reasonable bounds for our k value (e.g. 3.8 s^{-1}<k<28.3 s^{-1}).

With k and f_1 selected, the general range of h_1 and h_2 can be constrained with Eqn. 6 and Eqn.7. In simultaneously trying to minimize the error of estimated values of u_{eff} and D (in comparison to values determined from fitting to observations), we overlay two-dimensional surfaces (axis of h_1 and h_2)of residual error estimates for u_{eff} and D to determine the region of minimal error for both u_{eff} and D from which to select possible h_i values. Since we can only establish a range of possible k values, we repeat this determination of h_i values several times for different k. Several fits for different k and the corresponding h_i values are shown in Figure 3.5. The lowest k value (k=5 sec^{-1}) results in too much dispersion from the leading edge but both k=10 and k=15 result in physically reasonable fits.

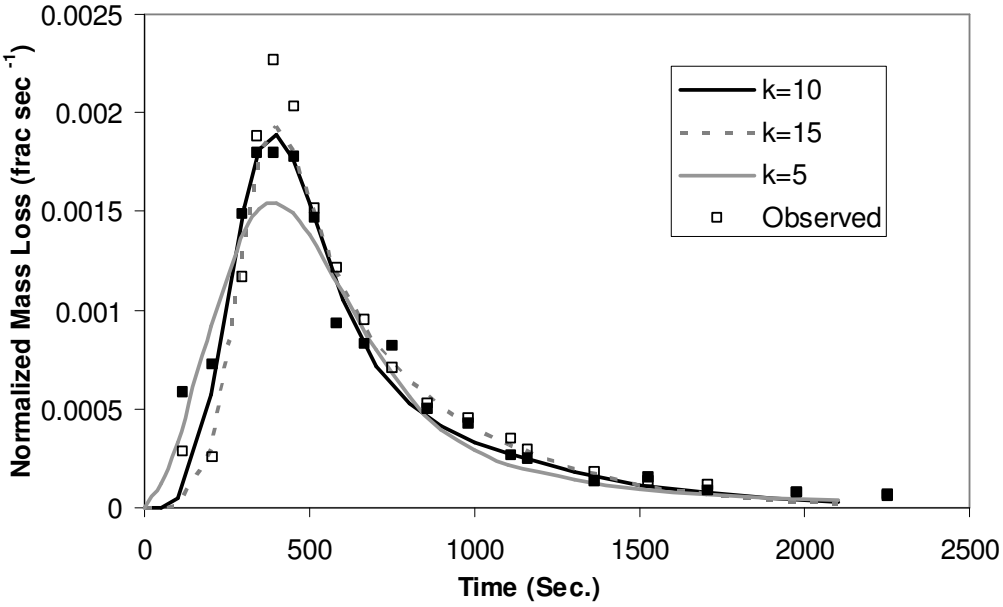

Figure 3.5. Comparison of 2-bin model fit to Surface 2 observations (filled and open symbols) with f_1=0.96. h_i's have been adjusted to counteract change in k. All three variations fit reasonably well with just k=5 resulting in slightly too much movement off the front edge.

Relating h to Drop Impact Area

While selected largely by calibration thus far, the ejection rate value, h, can also be attributed a physical meaning. As per Eqn. 3, h is the ratio of the impact area (A_i) of a single rain drop to the drop volume (V) scaled by the precipitation rate. Experiments by Mihara (1952) on sand indicated that the impact area was slightly larger than the drop diameter. So, outside of the deep cavities, we would expect A_i to be approximately 0.16 cm, the drop diameter. With h_1=0.045 s^{-1} for P=0.23 cm min^{-1} and a V of 2.1x10^{-3} cm^3 (assuming a spherical drop), we find A_i to be 0.18 cm, nearly the drop diameter. This suggests that shallow cavities do little to constrain the drop impact and that drop effectiveness is largely a function of the drop itself. Conversely, for the deep cavities with high retention (h_2=0.003 s^{-1}) classified by a diameter of <0.40 cm and a depth of >0.20 cm, the cavity depth appears to combine with the cavity diameter to constrain A_i to ~0.045 cm. Although the cavity diameter (~2 mm) is still larger than the drop diameter, the small A_i for these deep cavities suggests additional energy must depleted in overcoming the 2+ mm depth. Using this approach, h values could potentially be estimated *a priori* in future applications of the model.

Model Predictions for Full Surface Coverage

A more realistic test of the model would be a larger, plot scale, reach with complete initial particle coverage, not just a pulse. Experiments by Sansalone et al. (1998) reported particle counts /ml for 5 µm particles collected 9, 14, 24, 28, and 47 minutes after the start of a storm event on a 20 meter reach of roadway, thus providing a suitable data set for validating the model at larger scales. A three bin MRMT model with P =0.03 cm min^{-1}, minimal upslope inflow, a length of 20 m, V_{set} = 0.5 cm min^{-1}, and initial mass of 0.001 g cm^{-2} was compared to the observations (Figure 2.6). k was calculated assuming quiescent settling using the Stokes velocity for a 5 µm particle. h

and f_i parameters are summarized in Table 3.1. The three-bin model was implemented using a finite difference scheme in Matlab (Δt=0.25 min). The collection time of the Sansalone data points was shifted forward by 8 minutes to reflect the start of high intensity rainfall. Also note, since the Sansalone et al. (1998) data were only in terms of particle counts and the three bin MRMT model predicts mass loss, loss rates are reported as the ratio of loss at a given time to the maximum observed loss.

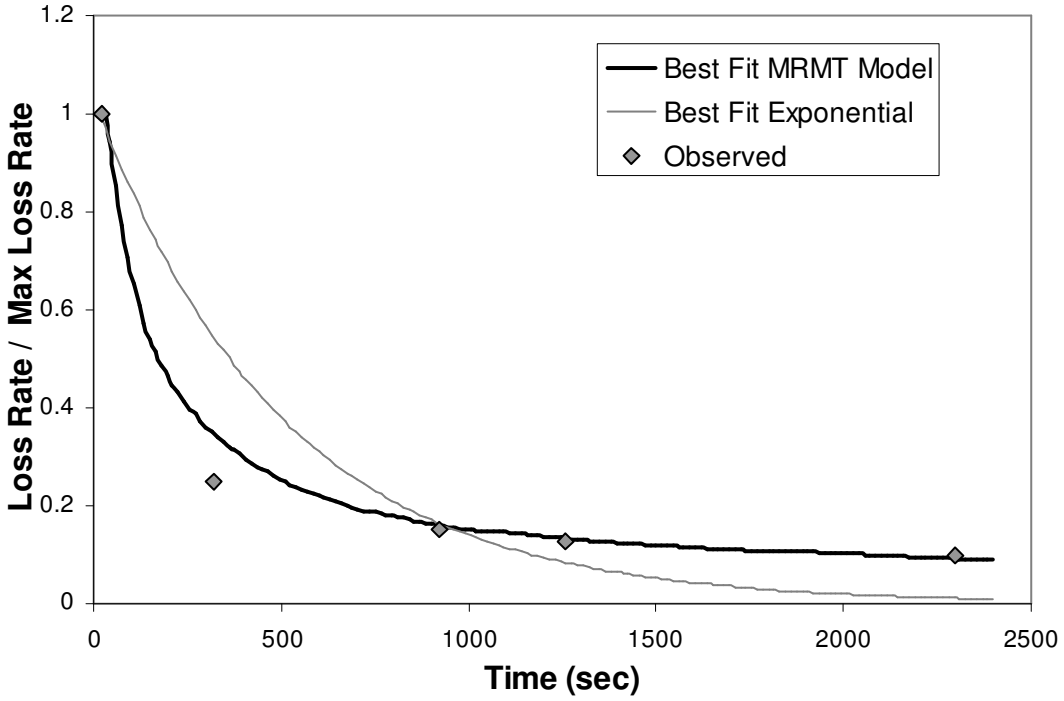

Figure 3.6. A three bin MRMT model (bold line) is applied to a 20 m reach with P=0.03 cm min^{-1} , minimal upslope inflow, 5 μm particles, and complete initial coverage of 0.001 g cm^{-2} . Model parameters are summarized in Table 1. The MRMT simulation is compared to wash-off observations for similar conditions published by Sansalone et al. (Fig.8 1998) as well as a. lumped exponential model (loss rate of 0.06 cm^{-1} and initial mass of 20 g).

Thus, while not assessing absolute mass loss rates, Figure 3.6 shows that the MRMT model is able to replicate the rapid peaking and then gradual tailing of the observed

mass loss. We presume that this initial peak results from particles near the bottom of the reach that do not fall into any deep surface cavities before exiting the system. Also shown in Figure 2.6, as a point of comparison, a lumped exponential model - traditionally used to predict wash-off – fails to predict the observed pattern of mass loss, greatly overpredicting the time at which the initial surface mass is exhausted. The rapid decline to a near zero loss rate by the exponential model is dramatically different considering we are looking at ratios of loss; the observed rate declines by ~80%, but the exponential declines by nearly 99%, significantly different in terms of actual mass loss.

3.6 Conclusions

To date, no urban pollutant transport models have addressed the role of surface roughness in retaining and attenuating particulate matter. We used a 2-bin MRMT to incorporate the effects of roughness into a physically-based wash-off model and found that model parameters could be related to characteristics of the impervious surface. The concept is demonstrated at the laboratory scale as well as compared to previously published data from a 20 meter asphalt reach. With a small fraction of surface area having a long particle retention time, we can explain the dual behavior of a first flush followed by more steady, non-mass limited loss later in the storm, contrary to the behavior of an exponential wash-off model. At larger scales, where shear induced wash-off is more likely to dominate, the exponential model may still be reasonable. These insights could lead to improved design and placement of water quality management structures in urban landscapes.

Additionally, this investigation provides an interesting case study of a situation in which a standard, textbook model appears reasonable (the Fokker-Planck equation),

but a more physically accurate conceptual model can be slightly better fit and, more importantly, provide greater physical insight into the underlying processes. A similar revelation was made in regards to river systems in considering the use of dead-zone mixing models (Green et al. 1994) in place of a Fokker-Planck formulation. In this case, with just the two-bin MRMT model, we see most "dispersion" is actually due to variation in effective particle velocities as we do not include an explicit dispersion term. Additionally, we find that the asymmetrical "high-shoulder" of the receding limb of the breakthrough curve is likely due to the combination of two distinct particle velocity distributions and not just an experimental anomaly.

REFERENCES

Alley, W.M. 1981. Estimation of Impervious Area Wash-off Parameters. Water Resources Research. 17(4):1161-1166.

Akan, A.O. 1988. Pollutant Washoff by Overland Flow. Journal of Environmental Engineering. 113(4): 811-823.

Anderson, D.A., R. S. Huebner, J.R. Reed, J.C. Warner, and J.J. Henry. 1998. Report prepared for National Cooperative Highway Research Program. Improved Surface Drainage of Pavement. NHCRP Web Document 16. National Academy of Sciences.

Chen, J and BJ Adams. 2007. A derived probability distribution approach to stormwater quality modeling. Advances in Water Resources, 30, 80-100.

Cristina, C. M. and J.J. Sansalone. 2002. Kinematic Wave Modeling of Pavement Rainfall-Runoff Subject to Traffic Loadings. Journal of Environmental Engineering, 129(7): 629-637.

Deletic, A., C. Maksimovic, and M. Ivetic. 1997. Modelling of Storm Wash-off of Suspended Solids from Impervious Surfaces. Journal of Hydraulic Research. 35(1): 99-117.

Deng, Zhi-Quiang, J.L.M.P. de Lima. and V.P. Singh. 2005. Fractional Kinetic Model for First Flush of Stormwater Pollutants. Journal of Environmental Engineering. 131(2): 232-241.

Fischer, H.B., E.J. List, R.C.Y. Koh, J. Imberger, N.H. Brooks. 1979. Mixing in Inland and Coastal Waters. Academic Press, New York.

Green, H.M., K.J. Beven, K.Buckley, and P.C. Young. "Pollution incident prediction with uncertainty". In Mixing and Transport in the Environment, Ed. By K.J. Beven, P.C. Chatwin, and J.H. Millbank. Ch. 6, John Wiley and Sons, Chichester.

Haggerty, R. and S.M. Gorelick. 1995. Multiple-rate mass transfer for modeling diffusion and surface reactions in media with pore scale heterogeneity. Water Resources Research, 31(10): 2383-2400. :

Hairsine, P.B. and C.W. Rose. 1991. Rainfall Detachment and Deposition: Sediment Transport in the Absence of Flow-Driven Processes. Soil Science Society of America Journal. 55: 320-324.

Lisle, I.G., C.W. Rose, W.L. Hogarth, P.B. Hairsine, G.C. Sander, and J.-Y. Parlange. 1998. Stochastic Sediment Transport in Soil Erosion. Journal of Hydrology, 204: 217-230.

Macklin, W.C. and G.J. Metaxas. *1976. Splashing of Drops on Liquid Layers.* Journal of Applied Physics 47(9): 3963-3970.

Mihara, Y., 1952. Raindrop sand Soil Erosion, Bulletin 1, Nat. Inst. Agric. Sci., Tokyo, Japan. Cited in: Al-Durrah, M.M., and J.M. Bradford. 1982. The mechanism of raindrop splash on soil surfaces, Soil Sci. Soc. of Am. J., 46: 1086-1090.

Nino, Y., F. Lopez, and M. Garcia. 2003. Threshold for particle entrainment into suspension. *Sedimentology*, 50, 247-263.

NOAA. 1977. Five to 60-Minute Precipitation Frequency for the Eastern and Central US. NOAA Technical Memorandum NWS HYDRO-35, Silver Spring, Md.

Oberhettinger, F. and L. Badii, *Tables of Laplace Transforms*, Springer, New York, 1973.

Parsons, A.J. and S.G.L. Stromberg. 1998. Experimental analysis of size and distance of travel of unconstrained particles in overland flow. *Water Resources Research*, 34:2377-2381.

Pedit, J.A. and C.T. Miller. 1994. Heterogeneous Sorption Processes in Subsurface Systems: 1. Model Formulations and Applications. Environmental Science and Technology. 28:2094-2104.

Potter, K. 2006. Small-scale spatially distributed water management practices: Implications for research in the hydrologic sciences. Water Resources Research. 42, W03S08.

Sansalone, J.J., J.M. Koran, J.A. Smithson, and S.G. Buchberger. 1998. Physical Characteristics of Urban Roadway Solids Transported During Rain Events. Journal of Environmental Engineering. 124 (5): 427-440.

Shaw, S.B., M.T. Walter. T.S. Steenhuis. 2006. A Simple Model of Wash-off from Urban Impervious Surfaces. Journal of Hydrology, 372: 618-626.

Shaw, S.B., R. Makhlouf, M.T. Walter. J.-Y. Parlange. 2007. Experimental Testing of a Stochastic Sediment Transport Model. Journal of Hydrology (in press).

Tsihrintzis, V. and R. Harmid. 1998. Runoff quality prediction from small urban catchments using SWMM. Hydrological Processes. 12:311-329.

Wang, P.P., C. Zheng, and S.M. Gorelick. 2005. A general approach to advective-dispersive transport with multirate mass transfer. Advances in Water Resources, 28: 33-42.

Van Genuchten, N. Th., and R.J. Wagenet, 1989. Two-site, two-region models for pesticide transport and degradation: theoretical development and analytical solutions. Soil Science Society of America Journal. 53 (5): 1303-1310.

Vaze, C. and F.H.S. Chiew. 2003. Study of Pollutant Washoff from Small Impervious Experimental Plots. Water Resources Research. V. 39(6): pp HWC 3-1 to 3-9.

Chapter 4

Evaluating Urban Pollutant Build-up/Wash-off Models Using a Madison, Wisconsin Catchment

4.1 Abstract

Build-up/wash-off (BUWO) models are widely used to estimate particulate mass loss from urban watersheds. However, our analysis suggests that particulate wash-off during a storm event is little influenced by the number of dry days preceding the event (T_{dry}), casting doubt on the fundamental assumption motivating the use of BUWO models. Our analysis employed total suspended solids and discharge data for storm events collected by the USGS from 21 storm events during non-snow periods for a 9 km^2 suburban catchment in Madison, Wisconsin, in conjunction with National Weather Service NEXRAD radar reflectivity that described spatially and temporally variable kinetic energy inputs during storm events. We found that storm event runoff volume and rainfall kinetic energy explained 81% of the variability in particulate event particulate load; volume alone explained 69% of the variability in event loads. Time between storm events was not significant and added little to R^2. Additionally, we simulated storm event particulate loads using both a BUWO model (dependent on T_{dry} and event volume) and a model assuming a constant mass available for wash-off (dependent only on event volume). We identified the region within which a three parameter BUWO model behaves like a one-parameter constant mass model. The parameter sets for three BUWO models calibrated for different watersheds and reported in the literature all fell in this region. It appears that BUWO models have been calibrated to behave like a simple model with constant mass availability. As long as event volume explains a large portion of the variation in particulate load and other

factors such as rainfall kinetic energy are minor, we suggest that in many cases a constant mass model would provide a suitable and relatively accurate estimate of particulate wash-off.

4.2 Introduction

Runoff from urban and suburban areas often transports pollutants including nutrients, heavy metals, and pathogens to nearby water bodies (USEPA 1983). A large fraction of these pollutants are associated with particulate matter (Sansalone and Buchberger 1997, Vaze and Chiew 2004). A clear understanding of sources and processes affecting particulate transport can aid in developing practices to reduce particulate export to surface waters (Vaze and Chiew 2004).

Particulate pollutant loss in urban and suburban catchments has been calculated using simple Event Mean Concentration (EMC) models and by using more sophisticated build-up/wash-off (BUWO) models. An EMC model assumes a single flow weighted concentration can be used across an entire storm event (Charboneau and Barrett 1998). However, because the EMC may change between storms (Driscoll 1986, US EPA 1983), load predictions for unmonitored events can be inaccurate. To try to account for EMC variations between storms, urban BUWO models have been formulated to predict particulate loads as functions of the particle mass that has built-up on the surface between storm events (for example, Chen and Adams 2007). BUWO models are a standard feature of widely used water quality models such as the Storm Water Management Model (SWMM) (Huber and Dickinson 1988). However, SWMM can include many other processes (for example, Tsihrintzis & Hamid 1998), and the presumed BUWO processes are seldom assessed against internal, subcatchment scale observations.

Other work has questioned whether accounting for build-up can actually explain variations in washed-off particulate load. Sutherland and Jelen (2003) note that Sartor and Boyd (1972) – the work on which the build-up assumption is based – forced mass accumulation to pass through the origin at zero days antecedent build-up, exaggerating the degree to which accumulated mass increased over time during interstorm periods. They conclude that residual particulates are most likely always present on urban surfaces. Charboneau and Barrett (1998) related antecedent dry days (a typical proxy for the amount of build-up) to particulate load for eight sites in Austin, Texas, and found no trend. In evaluating wash-off models against a data set from Australia, Vaze and Chiew (2003) assumed all wash-off events started with the same available surface mass, effectively assuming surfaces have a relatively constant available mass. From other work in Australia, Egodawatta et al. (2007) measured total particulate mass available on urban surfaces before storm events and found similar wash-off quantities even with different amounts of particulate initially available . Finally, in adding a factor to account for antecedent dry days to a linear, multi-factor wash-off model, Soonthornnonda and Christensen (2008) increased the R^2 between observed and estimated TSS loads from 0.23 to 0.38, based on 411 storm events in urban watersheds near Milwaukee, Wisconsin. While this is a moderate increase in R^2, the overall explanatory power of the model remained small.

We have two primary objectives for this paper. First, given that build-up has frequently been employed to explain interstorm variability in particulate load, we offer alternate factors to describe this variability, including kinetic energy. Kinetic energy has long been included in soil erosion models (see Wischmeier & Smith 1958). Only recently have researchers recognized that kinetic energy may be useful in predicting

particle wash-off in urban areas (Vaze and Chiew 2003, Egodawatta et al. 2007, Brodie and Rosewell 2007). Because rainfall kinetic energy is a nonlinear function of spatially and temporally variable rainfall intensity, standard aggregate measures such as discharge, total runoff volume, and average intensity may not reveal differences in kinetic energy. We make use of National Weather Service NEXRAD radar to assess high resolution rainfall patterns (approximately 1 km^2 grid size, 5 min. time interval). Investigators have used spatially variable rainfall in hydrologic models (Ogden et al., 2000, Smith et al 2005, Kalin and Hantush 2006) and spatially variable erosion models with uniform rainfall (Jain et al 2005), but the two have not generally been combined. Cruse et al. (2006) combined NEXRAD radar with the WEPP erosion model to predict daily erosion across Iowa, but the model was not compared to actual measurements of soil loss in streams.

Our second objective is to evaluate if the complexity of the build-up/ wash-off model is even necessary. We suggest that in many cases where available particulate for wash-off does not become depleted (i.e. a relatively constant supply of particulate is available), the particulate load estimated by a build-up model is predominantly determined by the event runoff volume. As long as the model can reproduce runoff volume, the event load will also be reasonable. A simulation study demonstrates that for common parameter values the BUWO model behaves like a model assuming constant particulate mass.

This paper is organized as follows. The next section introduces background on BUWO models. The third section discusses the methods of data collection and compilation. A fourth section evaluates kinetic energy and other variables in regression models for explaining interstorm variability in particulate load. A fifth section considers when

BUWO models behave like a model with constant mass. The two final sections provide discussion and conclusions.

4.3 Model Background

There is no standard way to formulate BUWO models. However, variations among formulations are relatively minor and the conceptual basis remains the same. The basic model can be written:

$$M_{t+\Delta\tau} = M_t + \left\{ k \cdot \left(1 - \frac{M_t}{m_0} \right) - \alpha \cdot M_t \cdot q_t \right\} \Delta\tau_t \qquad (1)$$

where M_t (kg) is the available mass at time t, k is a build-up coefficient (kg time^{-1}), m_0 is the threshold at which additional mass does not accumulate on the surface (kg), q_t is runoff rate (m^3 time^{-1}), α is a wash-off rate constant (m^{-3}), and $\Delta\tau_t$ is the time increment. The subscript t indicates the quantities are unique to specific time periods. In Eqn. 1, particulate build-up (the second term on the right hand side) is assumed to accumulate asymptotically toward a maximum, m_0, (or decline to this equilibrium value if the initial conditions are above m_0) in the absence of wash-off. Wash-off (the third term on the right hand side) is assumed to occur linearly with q_t and M_t. To maintain the mass balance if the time step is large, an additional constraint is added so that mass loss cannot be greater than the amount on the surface at the beginning of a wash-off event.

A simplification of this build-up/ wash-off model would be a model assuming a constant mass (Eqn. 1 would reduce to $M_{t+\Delta\tau} = M_{avg}$). With constant mass, loss in each time step ($Loss_t$, equivalent to the third term on the right hand side in Eqn. 1) can be written:

$$Loss_t = \alpha \cdot M_{avg} \cdot q_t \cdot \Delta\tau_t \quad (2)$$

where M_{avg} is the modeled available mass which can be considered as the average M_t obtained with the BUWO model (Eqn. 1).

When $\Delta\tau$ becomes very small, Eqn. 1 can be configured as a pair of differential equations. For a period with no rainfall, Eqn. 1 becomes:

$$\frac{dM_t}{dt} = k\left(1 - \frac{M_t}{m_0}\right) \quad (3a)$$

Assuming build-up is negligible during storm events, the change in mass during a wash-off event becomes:

$$\frac{dM_t}{dt} = -\alpha M_t q_t \quad (3b)$$

The solution of these differential equations is frequently used exponential build-up and wash-off equations (e.g. Easton et al 2007, Chen & Adams 2007).

Build-up:

$$M_{t+T_{dry}} = M_t + (m_0 - M_t) \cdot \left(1 - \exp(-\frac{k}{m_0} T_{dry})\right) \quad (4a)$$

Wash-off:

$$Loss_{t+T_{dry}} = M_{t+T_{dry}} \left(1 - \exp(-\alpha V)\right) \quad (4b)$$

where T_{dry} is the number of days since a significant discharge event, and V (the storm volume) is the integration of q_t over the storm event duration. The *Loss* is subtracted from M_t before calculating the build-up during the next time interval of T_{dry}. The quantity k/m_0 in Eqn. 4a is often written as a single parameter which we denote as k^*. As long as Eqn. 1 is evaluated at short time steps, $\Delta\tau$, Eqn. 1 and 3 are fundamentally the same.

4.4 Methods

Site Description

In our analyses, we make use of total suspended solids (TSS) concentration data collected by the USGS at a storm drain outlet in Madison, Wisconsin (Spring Harbor Drain – USGS #5427965). The Spring Harbor catchment covers approximately 9 km^2 and consists primarily of suburban, residential land use. Watershed boundaries were approximated from USGS topographic maps. The soils consist of sandy and silt loams with saturated conductivities greater than 0.75 m day^{-1} and depths of at least 2 m (USDA NRCS web soil survey: http://websoilsurvey.nrcs.usda.gov/app/WebSoilSurvey.aspx). A network of drainage pipes conveys storm water in areas close to the outlet. Open ditches in the more distant regions of the catchment appear to connect into this pipe network.

Data

To assess the validity of BUWO models, we use a sequence of 19 storm events from May to November 2002. This includes all storm events during that period with a peak discharge exceeding 0.28 m^3 sec^{-1} (most events exceed at least 1 m^3 sec^{-1}) except for an event on 8/11/2002 for which limited suspended solids data was available. We use consecutive storm events to assure a complete history of particulate loss because wash-off from a storm event can be dependent on what remains after the previous events.

Seven of the 19 events lacked the National Weather Service radar data needed to calculate kinetic energy. Therefore, we only use 12 of those 19 storm events to assess the role of kinetic energy in explaining interstorm variability in loads. To these 12

storms, we added two 2001 storms to supplement the 2002 record, for a total of 14. Table 4.1 summarizes data from the 21 unique storm event used within this paper.

To calculate event loads from our observed data for each storm event, we first establish concentration-discharge (*C*-*q*) relationships with the form of a power law:

$$C_t = \omega q_t^{\eta} \tag{5}$$

where C_t is the total suspended solids concentration at a given time interval and ω and η are parameters. The *C*-*q* relationships for each storm event are calibrated by finding the intercept and slope of a least-squares regression line fitted to the log adjusted *C* and *q* values. As examples, *C*-*q* relationships from the first five storm events of 2002 are shown in Figure 4.1. Across all 21 events used in the analyses, ω varies between 0.4 and 15.1 with an average of 7.8, and η varies between 0.46 and 2.22 with an average of 1.1.

An event volume (V_i) is calculated as:

$$V = \sum_{t=0}^{T_{end}} q_t \Delta\tau_t \tag{6}$$

where $\Delta\tau_t$ is the time interval between discharge measurements, typically five minutes during rainfall and 15 minutes in the receding leg of the storm hydrograph. Because discharge is predominantly ephemeral in the Spring Harbor watershed, the start of most events is easily discerned. The event is considered to begin (t=0) at the rapid rise in the hydrograph after the initiation of rain and continues until the discharge drops to 0.04 m^3 sec^{-1} at some time T_{end}. If another storm event starts before the hydrograph drops to 0.04 m^3 sec^{-1}, T_{end} is set at the time of minimum discharge before the next event peaks.

Table 4.1. Data summary of the 21 storm events used in the two analyses. Radar data was not available for events without KE_{30} or I, as indicated by the dashes.

Date	L (mt)	V (m^3)	KE_{30} (kJ)	q_p (m^3 sec^{-1})	T_{dry} (days)	I ($cm\ hr^{-1}$)
5/1/2002	1.31	1.61E+04	--	0.91	3	--
5/9/2002	1.70	1.03E+04	291	0.40	8	3.34
5/11/2002	1.50	1.05E+04	1050	0.68	2	10.77
5/25/2002	1.64	2.38E+04	345	0.93	14	4.08
5/28/2002	15.70	1.73E+04	--	2.66	3	--
6/3/2002	12.00	5.33E+04	4570	4.31	5	35.36
6/4/2002	7.01	8.73E+04	--	2.04	1	--
6/10/2002	8.15	4.02E+04	9750	5.16	6	63.6
6/13/2002	0.80	4.28E+03	1520	1.70	3	14.18
6/26/2002	2.57	8.41E+03	2680	1.78	13	21.00
7/20/2002	1.50	8.10E+03	3350	2.72	24	32.07
7/22/2002	3.40	2.81E+04	179	2.83	2	2.28
8/13/2002	1.20	1.89E+04	--	1.13	2	--
8/17/2002	4.60	1.41E+04	4810	2.44	4	34.88
8/21/2002	12.60	2.42E+04	--	3.77	4	--
9/2/2002	3.30	3.82E+04	916	3.20	11	9.32
9/19/2002	0.29	7.88E+03	--	0.59	17	--
9/29/2002	0.57	1.31E+04	--	0.65	9	--
10/4/2002	6.28	6.91E+04	2810	5.16	5	24.13
7/17/2001	1.70	6.03E+03	1350	1.95	29	24.18
8/1/2001	6.12	2.61E+04	818	3.80	6	7.62

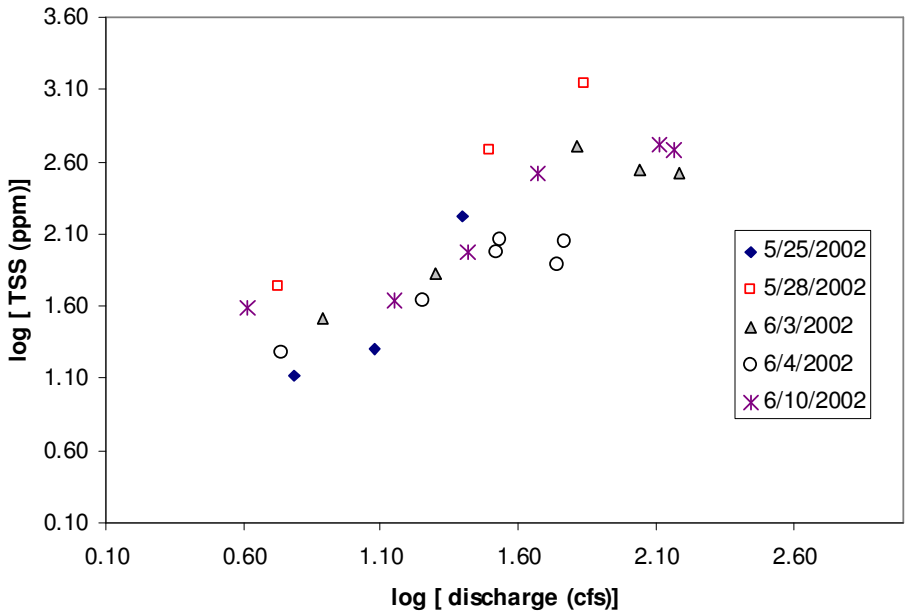

Figure 4.1. Relationships between discharge and TSS concentration for select storm events.

An event load (L) is calculated as:

$$L = \sum_{t=0}^{T_{end}} q_t C_t \Delta\tau_t \qquad (7)$$

where the function for C_t (Eqn. 5) is uniquely calibrated for each storm event.

For the 14 storm events with available radar data, we compiled time between storms (T_{dry}), total storm volume (V), kinetic energy (KE_{30}), and rainfall intensity (I_{30}). Table 4.2 provides a more extensive explanation of each variate. Here, I_{30} makes use of the high resolution radar data and is fundamentally different than an average rainfall intensity over a complete storm event.

Table 4.2. Summary of variables.

Variable	Description
I_{30}	rainfall intensity for 30 minute span before storm peak (cm hr^{-1})
k	loss rate in wash-off model
KE_{30}	sum of kinetic energy for 30 minute span before storm peak discharge (kJ)
L	storm event load (metric tons)
M_t	mass on surface in wash-off model (kg)
m_0	threshold at which additional mass will not accumulate in wash-off model (kg)
q_p	storm event instantaneous peak discharge (m^3 sec)
T_{dry}	time period without runoff prior to storm event (days)
V	storm event runoff volume (m^3)
α	build-up rate in build-up model

Converting from Radar Data to Kinetic Energy

No rain gauge data was available directly over the catchment so rainfall was instead estimated from radar reflectivity data. The radar data had the added benefit of providing greater resolution of spatial variations (~1 km^2) in rainfall intensity over the catchment than would be available from a limited rain gauge network, an important feature given the convective storm events of concern here. Radar reflectivity (mm^6 m^{-3}) is measured on a logarithmic scale in dBZ (decibels). When the radar is operating in

precipitation mode (in contrast to clear air mode), light rain corresponds to approximately 20 dBz (Rinehart 1991 p119). Of the 14 storm peaks we analyzed, our maximum observed reflectivity was 60 dBz.

Radar reflectivity data over the catchment was obtained from the National Weather Service Archive of WSR-88D NEXRAD Radar Data stored on the NCDC Robotic Mass Storage System (accessible at http://www.ncdc.noaa.gov/oa/radar/radardata.html). The closest station to our catchment was Milwaukee, Wisconsin (KMKX). Typically, we obtained Level 2 reflectivity data at 10 minute intervals from 40 minutes before to 10 minutes after each storm peak for a total of six images for each event analyzed. The raw Level 2 data were converted to a shapefile using the NCDC Java NEXRAD Data Exporter V. 1.3.5; only reflectivity at the lowest cut angle elevation was selected. Within ArcGIS, this base reflectivity was clipped to the approximate 9.4 km^2 catchment boundary and converted to a raster grid with 100 m square cells. From this grid, the distribution of reflectivity values at a given time interval was determined. Table 4.3 provides an example of the observed reflectivity and calculated kinetic energy and volume at each time interval for a storm event.

Reflectivity was converted to rainfall intensity (R, mm hr^{-1}) using a power law reflectivity-rainfall (Z-R) relationship ($R=aZ^b$ where Z is the reflectivity in mm^6/m^3). The Z-R relationship can vary among geographic regions and different storm event types, although Rinehart (1991 p 119) notes the variations are usually minor. Due to the limited rain gauge data within our catchment on which to optimize our choice of parameters, we use previously published Z-R relationships for convective storms (Smith et al. 2005). where a=0.0174 and b=0.71.

Table 4.3. Event data from a storm on 7/20/2002 (shown in Figure 4.2b.) Lines 2 through 13 in each column indicate the distribution of radar reflectivity values (Z) across the catchment at each give Central Standard Time (1510, 1520, etc.). The two bottom lines indicate total discharge volume and total kinetic energy for the time interval. Note, in the analysis, we only looked at radar on 10 minute intervals but here we look at 5 minute intervals around the peak (~1535) in order to better infer the delay between storm peak and discharge peak (1555).

	Z	1510	1520	1530	1535	1540	1545	1550	1600
# 100 m sq. cells at each Z (dBZ)	0	774	0	0	0	0	0	0	0
	5	165	62	0	0	0	0	0	0
	10	6	202	0	0	0	0	0	0
	15	0	316	0	0	0	0	0	0
	20	0	223	0	0	0	0	0	0
	25	0	30	0	0	0	0	0	0
	30	0	99	327	0	0	0	0	0
	35	0	0	22	0	0	0	100	0
	40	0	0	157	0	0	257	580	945
	45	0	0	439	153	0	522	175	0
	50	0	0	0	412	945	166	90	0
	55	0	0	0	380	0	0	0	0
Volume (m^3)		12	750	24,570	137,893	97,237	45,954	29,734	0
KE (kJ)		8.3E+01	9.8E+03	5.8E+05	4.3E+06	2.8E+06	1.2E+06	7.2E+05	4.0E+05

To evaluate the reasonability of this Z-R relationship in our catchment, we compared observed Spring Harbor gauge discharge summed up to 48 hours after a storm ended to the event rainfall as estimated from the radar. We used three brief, distinct (less than an hour) storms. For these three, two storms (8/17/2002 and 6/26/2002) had an estimated rainfall to observed discharge ratio of 0.090 and 0.094 (a ratio of 1 would indicate all rainfall was converted to observed runoff). For summer storms in a suburban catchment in Western New York, Easton et al. (2007) also observed that approximately 10% of rainfall was converted to runoff, suggesting that the power law relation is generally reasonable. A storm on 7/17/2001 had a ratio of 0.054, but that storm was proceeded by 29 days without significant rainfall (where 8/17/2002 and 6/26/2002 had 6 and 12 day dry antecedent periods, respectively). There are many sources of inaccuracy in rainfall estimates derived solely from radar reflectivity (Krajewski and Smith 2002 review the possibilities). Still, the estimates suit the

purposes of this paper: to evaluate a possible statistical relation between estimated kinetic energy and the actual observed wash-off in urban areas.

Rainfall intensity (I) (mm hr^{-1}) was converted to kinetic energy (KE) (kJ) using a power law relationship fitted to the data of Laws and Parsons (1943) by van Dijk. et al. (2002):

$$KE = 0.001 \cdot Area \cdot \kappa \cdot I^{n+1} \tag{8}$$

where κ=13, n=0.191, and $Area$ is the surface area (m^2) of each respective rainfall intensity grid cell. While many different functions relating intensity to kinetic energy have been proposed, recent work suggests that a power law is the most appropriate (Salles et al. 2002).

4.5 Explaining Interstorm Variability in Particulate Loads

Model Development

Potential predictor variables of L were evaluated in various regression models to predict L across the 14 storms with radar data in the Spring Harbor watershed. Vaze and Chiew (2003) observed that quantities ranging from total precipitation volume, total runoff volume, or average rainfall intensity have been used as the independent variable in wash-off models for predicting L. However, Vaze and Chiew (2003) noted the effects of any one quantity may be difficult to resolve because many variables are cross-correlated. Many quantities are inherently correlated to L due to the way in which L is calculated. As seen in Eqn. 6, L is dependent on the sum of a function of q over a storm event. Since precipitation drives runoff, the precipitation volume, total kinetic runoff volume, and average rainfall intensity will frequently be correlated with q and, consequently, L. A strong correlation resulting from the pairing of a variable

and a function of that same variable is referred to as a spurious self-correlation (see Kenney 1982, Vogel et al. 2005).

In Table 4.4, we consider the correlation between L and several independent variables in the 14 storm events. The correlation in the fifth column in Table 4.4 describes the explanatory value of the univariate regressions between L and either V, KE_{30}, q_p, or I_{30}. Because V is calculated as $\sum q_t \Delta\tau_t$ (see Eqn. 4.5) and L is also a function of q_t (Eqn. 6), the correlation between V ands L is relatively strong due to self-correlation, as elaborated on above. Additionally, the instantaneous peak discharge, q_p, is highly correlated to L. This is somewhat surprising considering that q_p is indicative of just a snapshot of the storm event. However, given the moderate correlation between q_p and V (r=0.80), it is likely that the most intense period of a storm event contributes a sizable amount to the total event V.

Table 4.4. Correlation coefficients (r) between L, KE_{30}, q_p, I_{30} and V.

	KE_{30}	q_p	I_{30}	L
V	0.32	0.80	0.26	0.76
KE_{30}	--	0.61	0.97	0.60
q_p	--	--	0.6	0.79
I_{30}	--	--	--	0.56

KE_{30} and I_{30} provide some slight explanation of variability in L. KE_{30} is highly correlated with I_{30} because KE_{30} is calculated from rainfall intensity at 10 minute intervals raised to the 1.2 power. We will use KE_{30} rather than I_{30} in the remainder of the paper because it provides marginally more explanatory power than I_{30}.

Consideration of Kinetic Energy

Rainfall kinetic energy's possibly explanatory value can be seen qualitatively by considering two events similar hydraulically (they have the same peak flow) but

differing in instantaneous concentration at the peak discharge. The event in Figure 4.2a has an instantaneous TSS concentration of 235 mg L^{-1} while that in Figure 4.2b has a concentration of 430 mg L^{-1}. Radar reflectivity maps for each event indicate different rainfall patterns; in this case, a narrow, high-intensity front in Figure 4.2b and a more expansive, slower moving storm in Figure 4.2a. KE_{30} is larger for the high-intensity front shown in Figure 4.2b (4.08×10^3 kJ) compared to the more diffuse storm event in Figure 4.2a (9.18×10^2 kJ), thus potentially explaining the difference in TSS concentrations.

More quantitatively, to identify the primary factors influencing particulate wash-off, we evaluate several model formulations for predicting L. Linear models relating $\ln(L)$ to $\ln(KE_{30})$ and $\ln(L)$ to $\ln(V)$ resulted in R^2 values of 0.19 and 0.69, respectively. However, a multivariate model:

$$\ln(L) = a + b \cdot \ln(V) + c \cdot \ln(KE_{30}) + \varepsilon \qquad (9)$$

resulted in an even better R^2 of 0.81. We have taken logarithms to achieve homoscedasticity among the errors, ε. Despite the fact that $\ln(V)$ explains much of the variation in the model given by Eqn. 9, the addition of $\ln(KE_{30})$ significantly adds to the prediction of $\ln(L)$ at the 2.4% level. Table 4.5 summarizes R^2 values, parameters, and p-values (calculated for a two-sided t-statistic) of the significance of each parameter within each model. Actually, a one-sided t-test can be justified because L should increase with both V and KE_{30}, allowing the p-values to be halved. Figure 4.3 shows the residuals associated with the three models; as would be expected, the model in Eqn. 9 consistently results in smaller residuals than $\ln(V)$ or $\ln(KE_{30})$ alone.

A model similar to Eqn. 9 in which KE_{30} is replaced by T_{dry} resulted in an R^2 value of 0.69 (model 5 in Table 4.5), the same result as using V alone (model 4 in Table 4.5).

For the Spring Harbor watershed, this result suggests that antecedent dry days play little role in explaining variability in *L*.

A model similar to Eqn. 9 in which KE_{30} is replaced by q_p (model 7 in Table 4.5) resulted in $R^2 = 0.77$; a statistical test on the *c* coefficient indicated that the addition of $\ln(q_p)$ barely adds to the prediction of $\ln(L)$ (*p*-value of 0.08 for a two-sided test). While the significance would frequently be rejected at the 5% level or less, the relatively small data set made us hesitant to dismiss the outcome outright.

Table 4.5. Summary of R^2, parameter values, and *p*-values of the significance of parameter coefficients for various linear regression models estimating $\ln(L)$. Dashes indicate the variable was not used in a given model. Within the row for each model, the top line contains the best-fit parameter values (standard error in parenthesis). The bottom line contains the *p*-value for the parameter.

Model	R^2	$\ln(T_{dry})$	$\ln(KE_{30})$	$\ln(q_p)$	$\ln(V)$	Intercept (a)
1	0.04	-0.18 (0.26)	--	--	--	1.49 (0.55)
		0.51	--	--	--	
2	0.19	--	0.29 (0.17)	--	--	-1.02 (1.28)
		--	0.12	--	--	
3	0.50	--	--	0.72 (0.21)	--	-2.03 (0.91)
		--	--	0.004	--	
4	0.69	--	--	--	0.75 (0.14)	-8.91 (1.93)
		--	--	--	0.0002	
5	0.69	-0.004 (0.16)	--	--	0.75 (0.15)	-8.88 (2.16)
		0.98	--	--	0.0005	
6	0.81	--	0.23 (0.09)	--	0.72 (0.12)	-10.14 (1.66)
		--	0.024	--	0.00009	
7	0.77	--	--	0.35 (0.18)	0.57 (0.16)	-8.03 (1.80)
		--	--	0.078	0.004	

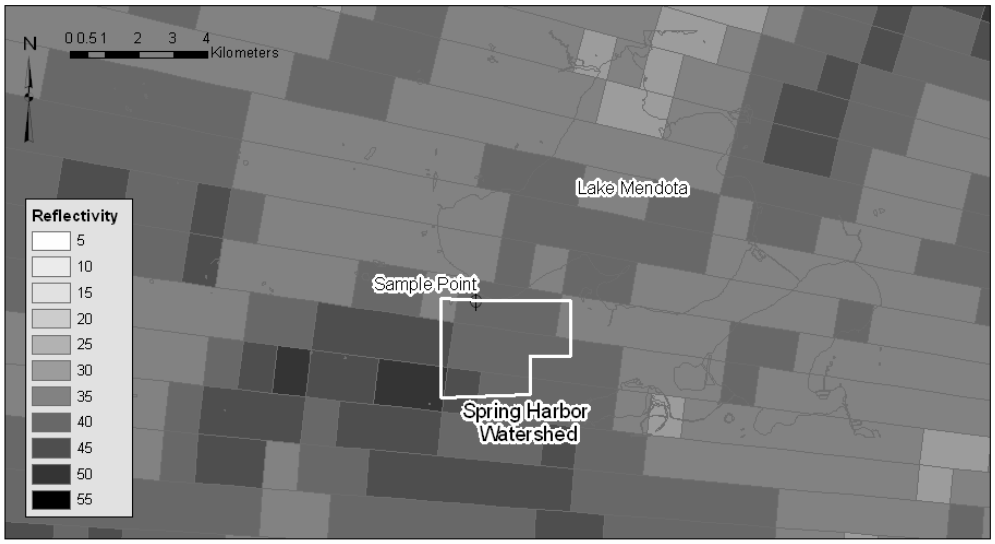

Figure 4.2a. NEXRAD reflectivity on 9/02/2002 at 0610 CST (central standard time). A TSS concentration of 230 mg $L^{-1}$was measured at 0620 CST at a peak discharge of 2.70 m^3 sec^{-1}.

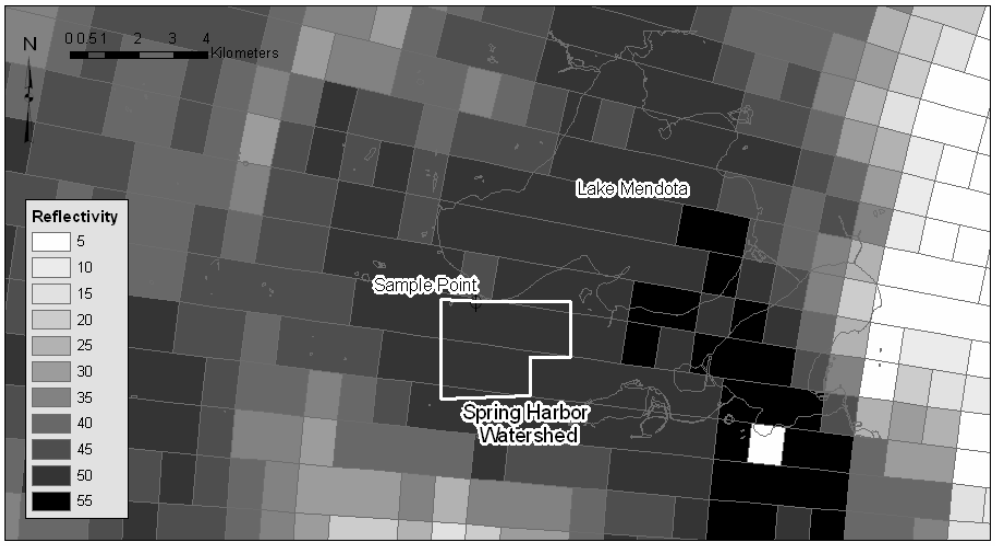

Figure 4.2b. NEXRAD reflectivity on 7/20/2002 at 1540 CST. A TSS concentration of 435 mg L^{-1} was measured at 155 CST at a peak discharge of 2.68 m^3 sec^{-1}.

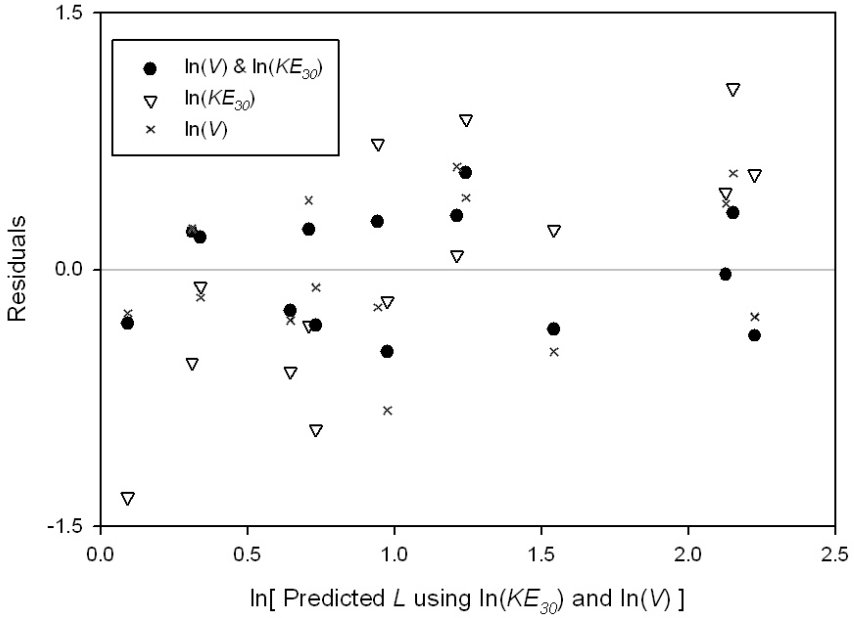

Figure 4.3. Residuals from three different regression models: a model including KE_{30} and V as variates (filled circles, R^2=0.81), a model only including KE_{30} (open triangles, R^2=0.19), and a model only including V (cross symbols, R^2=0.69).

However, given that q_p is moderately correlated to V (r=0.80, see Table 4.4), it is somewhat surprising q_p adds explanatory power beyond V. Additionally, as seen earlier in Table 4.4, q_p and KE_{30} are not highly correlated, suggesting that q_p results in improvements in models predicting L for different reasons than KE_{30}. A large q_p could possibly result from either intense rainfall (and sizable kinetic energy input) or wet antecedent soil moisture conditions. Obviously, higher intensity would enhance particulate loss but the role of wetter antecedent conditions on particulate loss is unclear. Therefore, certain changes in the magnitude of q_p may be unrelated to changes to L, resulting in its diminished predictive value in comparison to KE_{30} and the weak significance of q_p. This is seen in our qualitative example in Figure 4.2 where the same q_p is associated with different TSS concentrations.

4.6 Evaluation of BUWO Models

The regression models in the previous section suggested that the magnitude of particulate load in storm water is not explained by antecedent dry days (T_{dry}). However, BUWO models are specifically formulated to use T_{dry} to predict loads. Thus, we ask why BUWO models have proved suitable in application despite the failure of T_{dry} to predict loads (Charboneau and Barrett 1998, Sutherland and Jelen 2003, Vaze and Chiew 2003).

From the regression models we saw that L is closely correlated to V. A process model assuming constant available mass (e.g. Eqn. 2) functionally assumes all variation in L is dependent on V and none on T_{dry}. In this section we evaluate under what circumstances BUWO models could be simplified to a wash-off model with constant available mass (herein called the "constant mass model").

Applying a BUWO Model to the Spring Harbor Catchment

Here, we compare the particulate loads estimated directly from a BUWO model (Eqn. 1) and constant mass model (Eqn. 2) to observed loads from the 19 near-consecutive storms in the Spring Harbor watershed. Compared to the regression models, this is a more rigorous assessment of the role of antecedent dry days because the BUWO model accounts for the full history of the BUWO sequence. T_{dry} in the regression models only reflects the time since the last storm event occurred and does not account for the magnitude of the previous rain even. Large storms may have been preceded by very small storms that reset T_{dry}, but which did not remove a large amount of particulate.

Using a nonlinear fitting routine in Matlab (Mathworks Inc.), we found that neither the BUWO model nor the constant mass model could explain variability in L any better than assuming a constant loss from each storm event. The largest observed event loads (the events on 5/28/02 and 8/21/02 in Table 4.1) correspond to neither the largest discharge volumes nor the longest duration as represented by T_{dry}, the only drivers on which the models are dependent. This outcome is somewhat surprising considering the relatively strong link between V and L found in Section 4. However, radar data was not available for the two anomalous events (5/28/02 and 8/21/02). These storms may be instances where KE_{30} or some other unidentified factor is critically important to estimating L.

In the remainder of this section, we assess when the BUWO models reported in the literature (Chen and Adams 2007, Easton et al. 2007, Butler and Adams 2000) are indistinguishable from constant mass models.

Relating Constant Mass and BUWO Models

To obtain more general insight into similarities in output from BUWO and constant mass models, we compare various model parameterizations to determine when the BUWO and constant mass models may generate similar load predictions. Specifically, we calculate the correlation (r) between output from BUWO and constant mass models for a range of k^* and $\alpha \cdot E[Q_A]$ values selected from the literature (Chen and Adams 2007, Easton et al. 2007, Butler and Adams 2000), where $E[Q_A]$ is the average daily runoff amount over a year ($E[Q_A] = \sum q_t \Delta\tau_t / \sum \Delta\tau_t$). We use k^* (instead of just k) to make the comparison independent of m_0. In essence, m_0 scales the absolute magnitude of the wash-off and build-up processes, but m_0 is not important in assessing the correlation between BUWO and constant mass models. We use $\alpha \cdot E[Q_A]$ (instead

of just α) because it is a more general parameter accounting for possible compensating effects between α and $E[Q_A]$ across different watersheds (e.g. a wet region with a small α may be equivalent to a dryer region with a higher α). .

We evaluated 300 unique sets of k^* and $\alpha \cdot E[Q_A]$ for both the BUWO (Eqn. 1) and constant mass (Eqn. 2) models using the historical discharge time series from the Spring Harbor catchment as the driver. For each of the 300 paired simulations, the constant mass model (Eqn. 2) uses the same α as the BUWO model; the constant mass model is independent of k^*. (Note, because we are only evaluating the correlation between models, the constant mass model does not even actually need α specified). The correlation r was calculated on the loads estimated by the BUWO and constant mass models for the 19 summer storm events during 2002 in the Spring Harbor catchment. For the Spring Harbor catchment, $E[Q_A] = 1.12$ mm day^{-1}.

Figure 4.4 shows contour lines of r for a plot of $\alpha \cdot E[Q_A]$ (day^{-1}) versus k^* (day^{-1}).The quantity k^* is the rate constant for particulate build-up. Given that storms in the Midwest occur about once per week, k^* of greater than one implies that particulate should nearly always build-up to the surface maximum, m_0, before the next storm. In such a case there would be little difference between a BUWO model and a constant mass model. As shown in Figure 4.4, when k^*>1 day^{-1}, r approaches 1.

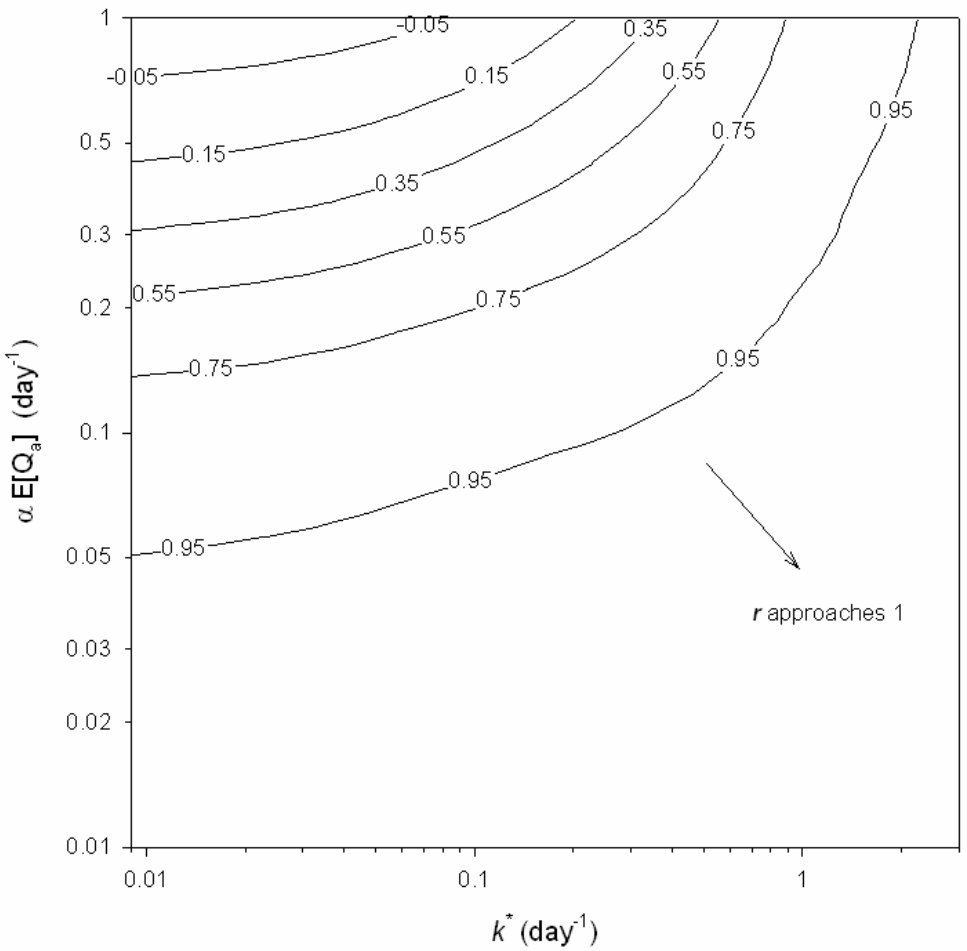

Figure 4.4. Correlation (indicated by the isolines) between storm event particulate loads estimated from constant mass (Eqn. 2) and BUWO models (Eqn. 1) for a range of k^* and $\alpha \cdot E[Q_A]$ values. The model simulations are driven by 2002 discharge data from the Spring Harbor catchment, Madison, Wisconsin.

The quantity $\alpha \cdot E[Q_A]$ is the rate constant of average daily particulate loss. $\alpha \cdot E[Q_A]$ can be large when either α or $E[Q_A]$ is large. Large $E[Q_A]$ results from sizable annual runoff due to either frequent rainfall or a high density of impervious surface in the catchment. Alternatively, large α implies the surface readily loses particulate. If $\alpha \cdot E[Q_A]$ is less than 0.1 day^{-1}, there is little loss with each storm event and available particulate remains near an equilibrium value. In this case, again, there would be little

difference between a BUWO model and a constant mass model. As shown in Figure 4.4, when $\alpha \cdot E[Q_A] < 0.1$ day^{-1}, r approaches 1.

When $\alpha \cdot E[Q_A] > 0.1$ day^{-1}, event loss becomes sizable and the available particulate mass can vary greatly between storm events. Only if k^* is commensurately increased will mass recover enough between storms so that the available mass at the beginning of each storm event remains relatively constant. Thus, to keep the same r with an increasing $\alpha \cdot E[Q_A]$, one must also increase k^*, as seen in Figure 4.4. We provide an illustration of this interplay between k^* and $\alpha \cdot E[Q_A]$ in Figure 4.5.

Figure 4.5 presents the magnitude of M_t over time for three different parameterizations of the BUWO model. The key feature to look at in each time series is the magnitude of M_t just before a downward drop marking a wash-off event. For the simulation resulting in r =0.85 (k^*= 0.03 day^{-1}; $\alpha \cdot E[Q_A]$= 0.12 day^{-1}), the pre-event M_t remains relatively close to 5 kg. Keeping k^* constant and increasing $\alpha \cdot E[Q_A]$ results in a simulation of r=0.23 (k^*= 0.03 day^{-1}; $\alpha \cdot E[Q_A]$= 0.40 day^{-1}) where the pre-event M_t fluctuates more widely. However, by increasing k^* to 0.58 day^{-1} while maintaining $\alpha \cdot E[Q_A]$= 0.40 day^{-1}, M_t fluctuations decrease and r=0.80. More quantitatively, the coefficient of variation of pre-event M_t values for the r=0.85 and r=0.80 simulations are 0.30 and 0.19 respectively while the coefficient of variation for the r=0.35 simulation is 0.57. This comparison of the coefficient of variation values clearly indicates greater relative variability in the pre-event M_t of the r=0.23 simulation.

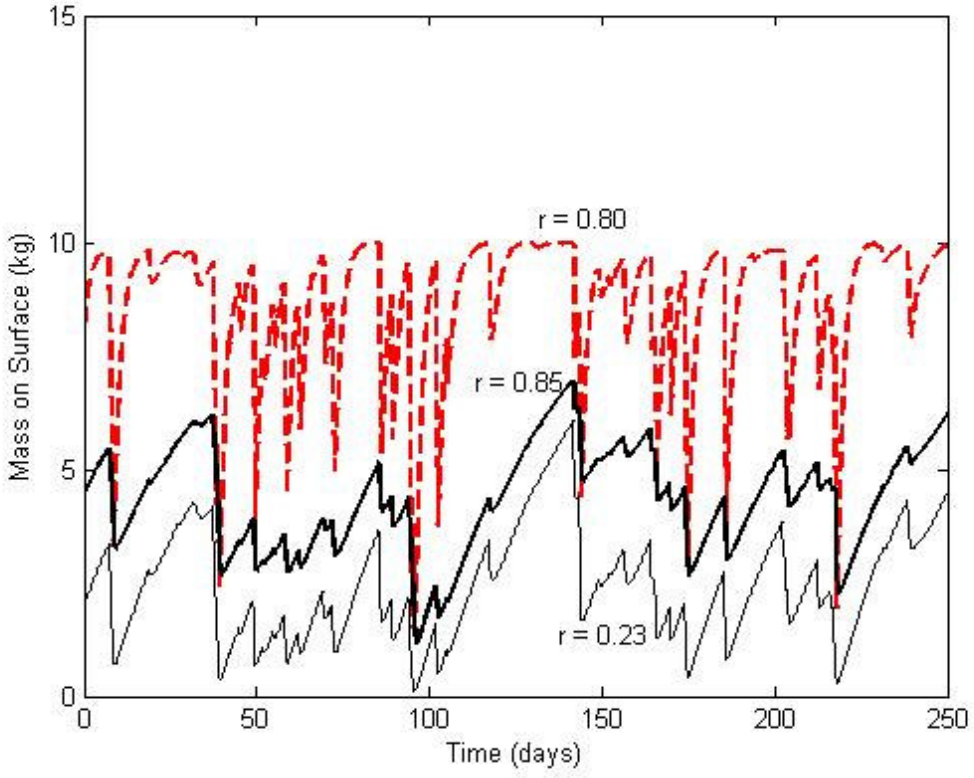

Figure 4.5. .Time series of M_t simulated using a BUWO model (Eqn. 1). The M_t represented by solid bold line (r=0.85) and the thin line (r=0.23) resulted from simulations with k^*=0.03 day^{-1} and $\alpha E[Q_A]$ = 0.12 and $\alpha E[Q_A]$ = 0.40 day^{-1}, respectively. The M_t represented by the bold dashed line (r=0.80) resulted from a simulation with k^*=0.58 day^{-1} and $\alpha E[Q_A]$ = 0.40 day^{-1}. Time zero corresponds to 3/2/2003.

Assessing BUWO Parameterizations in the Literature

We can use the relationships established in our Figure 4.4 contour plot to assess whether the use of BUWO models reported in the literature could have been replaced by simpler constant mass models. These models were of the continuous, exponential form (Eqn. 4). However, since Eqn. 1 and 3 are nearly equivalent when $\Delta\tau$ is small, we assume we can use the relationships in Figure 4.4 developed using simulations based on Eqn. 1 with $\Delta\tau$ between 5 and 15 minutes. Additionally, we assume the

arrival time of storms in these other watersheds is reasonably similar to that of the storm events in the Spring Harbor watershed.

Chen and Adams (Table 3, 2007) used k^*= 0.0245 day^{-1} and α = 0.0112 mm^{-1} for modeling TSS wash-off in Ontario, Canada (these parameters are referred to as*QFACT2* and *RCOEF*, respectively, in Chen and Adams 2007). The mean daily discharge was estimated as 0.40 mm day^{-1} (Chen and Adams 2007, Table 1 - mean rainfall and Table 2 - median runoff coefficient); resulting in $\alpha \cdot E[Q_A]$ = 0.044 day^{-1}. Evaluating against Figure 4.4, we find the combination of parameters is near the bottom of the chart, clearly in a range where *r* approaches one.

Butler and Davies (2000, p. 101) suggest ranges of k^* =0.2 to 0.4 day^{-1} and α = 0.1 to 0.2 mm^{-1} for use in Britain. Assuming 50% of the annual rainfall of 600 mm is converted to direct runoff in urban areas, $E[Q_A]$ is approximately 0.80 mm day^{-1}. The values of $\alpha \cdot E[Q_A]$ would range from 0.080 to 0.160 day^{-1}. Evaluating against Figure 4.4, the range of parameters used by Butler and Davies result in *r* values of 0.75 and greater.

Easton et al. (2007) used k^*= 6 day^{-1} and α=0.02 m^{-1} for modeling total dissolved phosphorus wash-off in central New York. While Easton et al. (2007) do not specifically model TSS, it is one of the few cases in the literature where the parameters associated with a BUWO model are fully reported, and we assume it is reasonably representative of how BUWO models are applied by others in practice. Based on pictorial information presented in Easton et al. (Figure 3, 2007), we assume a mean discharge of 0.010 m day^{-1}, thus $\alpha \cdot E[Q_A]$=0.0002 day^{-1}. Evaluating against

Figure 4.4, we find the combination of parameters is off the bottom of the chart in a range where *r* approaches one.

Thus, all three examples have parameters in a range where BUWO models generate similar output as constant mass models.

4.7 Discussion

A moderate amount of variability remains unexplained in the wash-off model given by Eqn. 9 (R^2 is 0.81). Additionally, unidentified processes limited our ability to model the sequence of 2002 storm events. These confounding factors may originate from a number of sources: sample mishandling, the finite number of samples used to construct rating curves for load estimates, failure of radar to represent actual rainfall kinetic energy at ground level, finer scale spatial and temporal variability than detected by the radar, or stochastic inputs of particulate matter.

We wish to elaborate more on this final error source – stochastic inputs of particulate - since it returns to the question of how and where materials build-up in urban landscapes. In particular, we do not necessarily believe that the available mass is truly constant on urban landscapes, despite the similarity between BUWO and constant mass models under certain parameterizations. Instead, we would suggest that build-up is not deterministically related to antecedent dry days. For instance, build-up is surely dependent on such unpredictable occurrences as construction work or the input of vegetative debris from strong storms. Build-up is unlikely to occur at a steady rate each day. Additionally, in a watershed with a storm drainage network, in addition to particulate build-up on surfaces such as pavement, there is likely to be temporary storage within pipes, catch basins, junction boxes, and other infrastructure (see Ashley

et al. 1992, Reeves et al. 2004). Flushing of this accumulated material is likely to depend on a complex interaction between the amount and composition of the stored material and hydraulic processes in the pipe network. Either unpredictable inputs or sporadic flushing of the pipe network could account for the large, unexplained loads, such as those seen in the sequence of 2002 storm events.

There is some question whether unpredictable inputs or sporadic flushing of pipes can ever be quantified sufficiently to be successfully included in a deterministic, process model. An evaluation of the uncertainty in a sewer water quality model applied in a watershed in Brussels found the model had no greater predictive capacity than the random drawing of pollutant concentrations from a probability distribution (Willems 2006). This suggests that if any kind of stochastic process is involved, one can only make reliable estimates over a time frame long enough to allow the stochastic inputs to converge to a relatively stable mean in the running average. Thus, an approach such as using event EMCs drawn from a specific probability distribution - many times labeled as a "planning methods" - may actually provide more reliable estimates than the supposedly more physically accurate, BUWO models.

If a modeler is confident that stochastic inputs are minor and wishes to construct a deterministic model to estimate event loads, new predictor variables will likely be needed because T_{dry} fails to capture the critical processes. Our analysis suggests that rainfall kinetic energy may be useful. Alternatively, as suggested by the correlation between KE_{30} and I (Table 4.4), high temporal resolution rainfall intensity data (at less than a one-hour time interval) could also be a suitable predictor variable. However, unlike T_{dry} which is readily calculated from the spacing between days with rainfall,

rainfall kinetic energy or intensity will require new data sets drawn from either NEXRAD radar or relatively rare, high resolution rainfall measurements.

4.8 Conclusions

We carried out two different analyses on a data set of TSS concentrations in storm water from a watershed in Madison, Wisconsin. First, by comparing several regression models, we found that the particulate load from storm events is best explained by the combination of event runoff volume and rainfall kinetic energy (R^2=0.81). Event runoff volume alone explained the majority of the variation in particulate load between events (R^2=0.69). Antecedent dry days, a traditional factor employed to explain variability in particulate load, had little explanatory value. The peak discharge in conjunction with runoff volume explained 77% of the variability in loads, but was only marginally significant (two-sided *p*-value=8%). It appears KE_{30} can potentially capture important differences in storm events not apparent from aggregate measures of storm events such as total volume, total rainfall, or average rainfall intensity.

As a second analysis, an extensive simulation study examined when a build-up/wash-off (BUWO) model yielded results similar to a constant mass model. We developed a contour plot relating k^* and $\alpha \cdot E[Q_A]$ to the correlation between BUWO and constant mass model losses to allow a simple assessment of whether build-up actually needs to be included in a BUWO model. We evaluated parameter sets from calibrated BUWO models for watersheds in Ontario, Canada; central New York; and Britain against our contour plot. For all three cases, the calibrated parameter values were in a range indicating that the BUWO models effectively functioned as constant mass models.

Despite various lines of evidence indicating T_{dry} has little value in explaining variation in particulate storm loads, build-up/ wash-off models are still widely used. Our limited assessment of build-up/ wash-off models suggests they have not been questioned by the engineers using them because they do not necessarily lead to unrealistic results. BUWO models have just been parameterized to behave similarly to a model with constant mass availability. As long as event loads are predominantly determined by event volume (a reasonable assumption as demonstrated with our regression models), particulate loss could be simulated with a one parameter constant mass model ($k \cdot M_{avg}$) instead of a three parameter model (k, α, and m_0). Such simplification is consistent with recent efforts to identify dominant processes (Sivakumar 2004) to avoid problems of equifinality and undue uncertainty in model predictions (Sivapalan et al. 2003). However, if one is interested in trying to better capture variability in event loads, our findings suggest that use of rainfall kinetic energy may be warranted, which is consistent with agricultural soil erosion models.

REFERENCES

Ashley, R.M., D.J.J. Wotherspoon, B.P Coghlan, and I. McGregor. 1992. The erosion and movement of sediments and associate pollutants in combined sewers. Water Science and Technology, 25(8): 101-114.

Brodie, I. and C. Rosewell. 2007. Theoretical relationships between rainfall intensity and kinetic energy variants associated with stormwater particle washoff. Journal of Hydrology, 340(1-2), 40-47.

Butler, D. and J.W. Davies. 2000. Urban Drainage. Taylor and Francis, 489 pp.

Charboneau RJ, and ME Barrett. 1998. Evaluation of methods for estimating stormwater pollutant loads. Water Environment Research, 70(7), 1295-1302.

Chen, J and BJ Adams. 2007. A derived probability distribution approach to stormwater quality modeling. Advances in Water Resources, 30, 80-100.

Cruse, R., D.Flanagan, J. Frankenberger, B. Gelder, D. Herzmann, D. James, W. Krajewski, M. Kraszewski, J.Laflen, J. Opsomer, and D.Todey. 2006. Daily estimates of rainfall, water runoff, and soil erosion in Iowa. Journal of Soil and Water Conservation.
61(4), 191-199.

Easton, Z.M., G.-P. Marchant, M.T. Walter, A. M. Petrovic, and T.S. Steenhuis. 2007. Hydrologic assessment of an urban variable source watershed in the northeast United States. Water Resources Research, 43, W03413.

Egodawatta, P., E. Thomas, and A. Goonetilleke. 2007. Mathematical interpretation of pollutant wash-off from urban road surfaces using simulated rainfall. Water Research, 41: 3025-3031.

Huber, W. C. and Dickinson, R. E. 1988. Storm Water Management Model, Version 4: Users Manual, EPA 600/3-88/001a. Environmental Research Laboratory, EPA, Athens, Georgia.

Jain, MK, Kothyari UC, Raju KGR. 2005. GIS based distributed model for soil erosion and rate of sediment outflow from catchments. Journal of Hydraulic Engineering – ASCE, 131(9), 755-769.

Kalin, L., M.M. Hantush. 2006. Hydrologic modeling of an Eastern Pennsylvania watershed with NEXRAD and raingauge data. Journal of Hydrologic Engineering, 11, 555-569.

Kenney, B.C., 1982. Beware of spurious self-correlations! Water Resources Research, 18(4), 1041-1048.

Krajewski, WF, and JA Smith. 2002. Radar hydrology: rainfall estimation. Advances in Water Resources. 25(8-12), 1387-1394.

Laws, J. O. and Parsons, D. A. 1943. The relation of rain drop size to intensity, Transactions of the American Geophysical Union, 24, 452-460.

Lee, J.H., and K.W. Bang. 2000. Characterization of urban stormwater runoff, Water Research, 34(6): 1773-1780.

Ogden, F.L., H.O. Sharif, S.U.S. Senarath, J.A. Smith, M.L. Baeck, J.R. Richardson. 2000. Hydrologic analysis of the Fort Collins, Colorado, flash flood of 1997, Journal of Hydrology, 228 (1-2): 82-100.

Reeves, R.L., S.B. Grant, R. D. Morse, C. M. Copil Oancea, B.F. Sanders, and A.B. Boehm. 2004. Scaling and management of fecal indicator bacteria in runoff from a coastal urban watershed in Southern California. Environmental Science and Technology, 38: 2637-2648.

Rinehart, R.E. 1991. Radar for Meteorologists. Rinehart, Grand Forks, ND.

Salles, C., J. Poesen, D. Sempere-Torres. 2002. Kinetic energy of rain and its functional relationship with intensity. Journal of Hydrology, 257 (1-4), 256-270.

Sartor, J.D. and G.B. Boyd. 1972. Water pollution aspects of street surface contaminants, U.S. Environmental Protection Agency (1972) EPA-R2-72-081.

Sansalone, J.J. and S.G. Buchberger. 1997. Partitioning of first flush metals in urban roadway storm water. Journal of Environmental Engineering, 123: 134-143.

Sivakumar, B. Dominant processes concept in hydrology: moving forward. Hydrological Processes, 18: 2349-2353.

Sivapalan, M., G. Bloschl, L. Zhang, and R. Vertessy. 2003. Downward approach to hydrologic prediction. Hydrological Processes, 17:2101-2111.

Smith, JA, ML Baeck, KL Meierdiercks, PA Nelson, AJ Miller, and EJ Holland. 2005. Field studies of the storm event hydrologic response in an urbanizing watershed. Water Resources Research, 41, W10413.

Soonthornnonda, P. and E.R. Christensen. A load model based on antecedent dry periods for pollutants in stormwater. Water Environment Research, 80(2): 162-171.

Sutherland, R.C. and S.L. Jelen. 2003. Stormwater quality modeling improvements needed for SWMM., Practical Modeling of Urban Water Systems Monograph 11, edited by William James, CHI Publications, 2003, pp. 253-289.

Tsihrintzis, V. and R. Harmid. 1998. Runoff quality prediction from small urban catchments using SWMM. Hydrological Processes. 12, 311-329.

Vaze, J., and F.H.S. Chiew. 2003. Comparative evaluation of urban storm water quality models. Water Resources Research, 39(10): 1280.

Vaze, J., and F.H.S. Chiew. 2004. Nutrient loads associated with different sediment sizes in urban stormwater and surface pollutants. Journal of Environmental Engineering, 130: 391-396.

Van Dijk, AIJM, LB Bruijnzeel, CJ Rosewell. 2002. Rainfall intensity – kinetic energy relationships – a critical literature appraisal. Journal of Hydrology, 261(1-4), 1-23.

Vogel, R.M., B.E. Rudolph, and R.P. Hooper. 2005. Probabilistic behavior of water-quality loads, Journal of Environmental Engineering, 131(7), 1081-1089.

Willems, P.2006. Random number generator or sewer water quality model? Water Science and Technology, 54 (6-7): 387-394.

Wischmeier, W.H. and D.D. Smith. 1958. Rainfall energy and its relationship to soil loss. Transactions of the American Geophysical Union. 39(2), 285-291.
.

APPENDIX

A. Chapter 2 – Experimental Observations

Run 1 (7/13/05)
P=0.10 cm min^{-1}
q= 300 mL min^{-1}
0.6 g initially appplied

	Mass Loss (g)	
Time (sec)	Rep. 1	Rep. 2
45	0.026	0.02
90	0.018	0.04
135	0.051	0.05
180	0.075	0.074
225	0.095	0.08
270	0.089	0.096
315	0.063	0.08
360	0.044	0.064
405	0.029	0.032
450	0.011	0.021
initial	0.013	0.03
rinse	0.015	0.028
Total	0.529	0.615

Run 2 (7/13-14/05)
P=0.15 cm min^{-1}
q= 300 mL min^{-1}
0.6 g initially appplied

	Mass Loss (g)		
Time (sec)	Rep. 1	Rep. 2	Rep. 3
45	0.036	0.004	0.011
90	0.031	0.023	0.035
135	0.070	0.073	0.128
180	0.092	0.108	0.116
225	0.070	0.106	0.089
270	0.045	0.09	0.041
315	0.018	0.043	0.017
360	0.014	0.021	0.013
initial	0.010	0.013	0.009
rinse	0.015	0.017	0.022
Total	0.401	0.498	0.481

Run 3 (6/30/05)
P=0.15 cm min^{-1}
q= 305 mL min^{-1}
8 g initially appplied

	Mass Loss (g)	
Time (sec)	Rep. 1	Rep. 2
45	0.989	0.991
90	1.400	0.857
135	1.310	1.092
180	0.769	1.154
225	0.645	1.102
270	0.601	0.797
315	0.625	0.503
360	0.340	0.412
405	0.269	0.219
450	0.111	0.117
initial	0.211	0.138
rinse	0.199	0.165
Total	7.469	7.547

B.1 Chapter 3 – Experimental Observations

Lot 2 (K Lot)

	Mass Loss (g)	
Time (min)	Run 1	Run 2
2.5	0.063	0.129
4.5	0.113	0.323
5.33	0.215	0.275
6.17	0.351	0.335
7	0.417	0.331
8.08	0.486	0.426
9.16	0.362	0.352
10.41	0.336	0.259
11.84	0.301	0.262
13.16	0.223	0.258
15.41	0.262	0.249
17.33	0.194	0.180
19.84	0.195	0.149
21.5	0.106	0.089
24	0.100	0.071
26.92	0.085	0.096
30	0.074	0.055
35.84	0.101	0.100
39.16	0.047	0.044
initial	0.295	0.210
rinse	0.146	0.150
Total	4.472	4.343

Lot 1 (RR Lot)

	Mass Loss (g)	
Time (min)	Run 1	Run 2
1	0	0
2	0.134	0.077
3.25	0.279	0.478
4	0.401	0.55
4.5	0.512	0.486
5.08	0.496	0.417
5.58	0.41	0.349
6.16	0.351	0.302
7	0.455	0.48
8.16	0.513	0.441
9.16	0.362	0.279
10.43	0.241	0.224
11.58	0.116	0.125
13.16	0.101	0.094
14.92	0.056	0.065
17.42	0.053	0.044
initial	0.176	0.06
rinse	0.033	0.049
Total	4.689	4.52

B.2 Chapter 2 – Matlab Code

```
%Analyt_R31 - A program to plot solutions to the Kolmogorv-Feller
Equations
%describing stochastic movement of a particle. The program makes use
of a
%solution determined by Lisle et al, 1998.
%Here we use a sum of convolutions to solve a double rate process.


x=.35; %m
T=2200;  %sec
dt=1;
dt2=5;
DT=50;

u=.1888;  %m/s
k=9.25;  %settling rate (1/sec) 17.2  20
h2=.038; %ejection rate (1/sec) with Kimpact=5   1.5
h3=.0021; %.15
f2=0.98;
f3=.02;


OutputTime=round(KTimeShift*60);
OutNum=length(OutputTime);

%Rate 1 Term-------------------------------------------------------------
--
for i=1:OutNum

    t=OutputTime(i);

    time(t)=t;

    if t<=(x/u)   % assures no uplsope flow
       t % counter
       p3(t)=0;
       r3(t)=p1(t)*u;
    else
        tau=h3*(t-(x/u));
        Epsi=k*x/u;

        Product=tau*Epsi*f1;
        BesselInput=2*realsqrt(Product);
        Bessel=mfun('BesselI',1,BesselInput);

       p3(t)=h3/u*exp(-Epsi-tau)*sqrt(Epsi*f3/tau)*Bessel;

       r3(t)=p3(t)*u;
    end  %if

end % for Rate 1
```

```
%Rate 2 Term-------------------------------------------------------------
---

for i=1:OutNum

    t=OutputTime(i);

    time(t)=t;
    if t<=(x/u)

       t
       p2(t)=0;
       r2(t)=p2(t)*u;
    else

        tau=h2*(t-(x/u)); %
        Epsi=k*x/u;

        Product=tau*Epsi*f2;
        BesselInput=2*realsqrt(Product);
        Bessel=mfun('BesselI',1,BesselInput);

       p2(t)=h2/u*exp(-Epsi-tau)*sqrt(Epsi*f2/tau)*Bessel;  %when tau
large, goes to zero as long as Bessel not infinite

       r2(t)=p2(t)*u;
    end  %if

end % for Rate 2

%Convolution 2/3----------------------------------------------------------
----
for i=1:OutNum
t=OutputTime(i);

      i=1;
      Convo_sum=0;
      for tau=1:dt:t+1

        if tau<=(x/u)+1
            Convo_sum=0+Convo_sum;

        elseif tau>=t-(x/u)+1     % removed -(x/u)

         Convo_sum=0+Convo_sum;

        else

        tau2=h2*((tau-1)-(x/u));
        tau3=h3*(t-(x/u)-(tau-1));   % removed -(x/u)
```

```
        Epsi=k*x/u;

        Product1=tau2*f2*Epsi;
        BesselInput1=2*realsqrt(Product1);
        Bessel1=mfun('BesselI',1,BesselInput1);

        Product2=tau3*f3*Epsi;
        BesselInput2=2*realsqrt(Product2);
        Bessel2=mfun('BesselI',1,BesselInput2);

        Convo_sum=h2*h3/u*exp(-Epsi)*exp(-tau2)*exp(-tau3)...
            *sqrt(Epsi*f2/tau2)*sqrt(Epsi*f3/tau3)...
            *Bessel1*Bessel2*dt+Convo_sum;

        end % elseif

      end  %for tau

      p23(t)=Convo_sum;
      r23(t)=p23(t)*u;

   end %for t Convolution 23


% Output-------------------------------------------------------------
---

% Observed
plot(KTimeShift*60,LossRateK1/60/3.7, 's');
hold on
plot(KTimeShift*60,LossRateK2/60/3.7, 's','MarkerFaceColor','k');
axis([0 T 0 .4e-2])
xlabel('Time (sec)');
ylabel('Nondimensional Mass Loss at L=35 cm (1/sec)');
%title('Breakthrough Curve for Lot 2 Surface');

% Model
for l=1:OutNum
    Output(l)=r2(OutputTime(l))+r3(OutputTime(l))+r23(OutputTime(l));
   Outputr2(l)=r2(OutputTime(l));
   Outputr3(l)=r3(OutputTime(l));
   Outputr23(l)=r23(OutputTime(l));
end

plot(OutputTime, Output,'k','linewidth',2);
plot(OutputTime, Outputr2,'g--');
% plot(OutputTime, Outputr3,'g--');
plot(OutputTime, Outputr23,'r--');
```

```
%MT_1_13_062
%Description:   Quantifies particulate wash-off from a rough,
impervious
%surface. Applied for scenario with >2 bins when analytical solution
%cannot be run efficiently.


% ---------------Constants----------------------------------

L=2000; % plane length (cm)
W=10; %plane width (cm)
Q=10; %inflow rate (mL/min)
Pq=15; % precip (mL/min)
P=Pq/10.5/60; %precip rate (cm/min)
P=.03;
RoM=.01; %initial particle spatial density in application area (g/cm)
.45

frac1=.70; %fraction of surface with shallow crevice .47
frac2=0.2; %.42
frac3=.1; %.11
a1=150; %drop effectiveness for crevice type 1 400
a2=20; %drop effectiveness for crevice type 2  25
a3=2; %drop effectiveness for crevice type 3  7

ddthresh=100*W*frac3*1.37;  %depth*width*ro*frac3  .05  why 1.37 -
bulk density
dthresh=100*W*frac2*1.37;  %.05

vset=.5; % settling veloc. (cm/min) 170 % 225 micron sand
f_thresh=100*W; %.03

dt=.0005; %.0002 time step (min) for .5 mm flow, .0004 sec settling
time (.00025)
T=40; % end time (min)
DT=.25; % reporting interval (min)

Time(1)=DT;
QMinP(1)=0;

%-------------Water Balance (dx determination)--------------

q(1)=Q;
i=1;
l=0;

while l<L
    [V(i),D(i)]=Mannings(q(i));
    dx(i)=V(i)*dt;
    l=l+dx(i);
    q(i+1)=dx(i).*P.*W+q(i);
    %q(i+1)=q(i);
    i=i+1;
```

```
end %while

TotalCells=i-1; %sets total number of cells in system

%---------Create Arrays-----------------------------------------


h=zeros(TotalCells,(DT/dt));
e1=zeros(TotalCells,(DT/dt));
e2=zeros(TotalCells,(DT/dt));
e3=zeros(TotalCells,(DT/dt));
Mg=zeros(TotalCells,(DT/dt+1));
Md=zeros(TotalCells,(DT/dt+1));
Mdd=zeros(TotalCells,(DT/dt+1));
Ms=zeros(TotalCells,(DT/dt+1));


%----------Initial Mass Distribution----------------------------------
----

i=1;
appL=0; %application zone length counter
MTot=0;

while appL<2000 % where 20 is application zone length
    Mg(i,1)=dx(i)*frac1*RoM;
    Md(i,1)=dx(i)*frac2*RoM;
    Mdd(i,1)=dx(i)*frac3*RoM;
    appL=dx(i)+appL;
    MTot=MTot+Mg(i,1)+Md(i,1)+Mdd(i,1); % a check on mass amount
applied - should be approx. 10 g
    i=i+1;
end %while

AppCells=i; % sets point at which cells have no initial application

j=0;
for j=AppCells:TotalCells
    Mg(j,1)=0;
    Md(j,1)=0;
    Mdd(j,1)=0;
end % for


%-----------Initial Suspended Mass Distribution (t=1)--------------

x=0;
for x=1:TotalCells
    Ms(x,1)=0;
end % for
```

```
%----Establish first set of initial values-------------------------

InitMs=Ms(:,1);   % changed 1 to 2
InitMg=Mg(:,1);
InitMd=Md(:,1);
InitMdd=Mdd(:,1);

%-----start interval calculations

i=1;
for i=1:T/DT

    i

    %------at x=1 for all t>1---------------------------------------
---

    Ms(:,1)=InitMs;
    Mg(:,1)=InitMg;
    Md(:,1)=InitMd;
    Mdd(:,1)=InitMdd;


    for t=2:(DT/dt+1)

    h(1,t)=vset*Ms(1,t-1)/D(1);
    if (h(1,t)*dt)>Ms(1,t-1)
        h(1,t)=Ms(1,t-1)/dt;
    end % if/else


    if Mg(1,t-1)>(f_thresh*dx(1)*frac1)
    e1(1,t)=a1*P*f_thresh*dx(1)*frac1;
    else
    e1(1,t)=a1*P*Mg(1,t-1);
    end

    if Md(1,t-1)>(dthresh*dx(1)*frac2)
        e2(1,t)=a1*P*f_thresh*dx(1)*frac2;
    elseif Md(1,t-1)>(f_thresh*dx(1)*frac2)
        e2(1,t)=a2*P*f_thresh*dx(1)*frac2;
    else
        e2(1,t)=a2*P*Md(1,t-1);
    end


    if (Mdd(1,t-1)/dx(1))>ddthresh
    e3(1,t)=a2*P*f_thresh*frac3*dx(1);
    elseif (Mdd(1,t-1)/dx(1))>(f_thresh*frac3)
    e3(1,t)=a3*P*f_thresh*frac3*dx(1);
    else
```

```
    e3(1,t)=a3*P*Mdd(1,t-1);
    end %if/else


    if (e1(1,t)*dt)>Mg(1,t-1)
        e1(1,t)=Mg(1,t-1)/dt;
    end % if/else

    if e1(1,t)<=0
        e1(1,t)=0;
    end

    if (e2(1,t)*dt)>Md(1,t-1)
        e2(1,t)=Md(1,t-1)/dt;
    end % if/else

    if e2(1,t)<=0
        e2(1,t)=0;
    end

    if (e3(1,t)*dt)>Mdd(1,t-1)
        e3(1,t)=Mdd(1,t-1)/dt;
    end % if/else

    if e3(1,t)<=0
        e3(1,t)=0;
    end

    Ms(1,t)=(.5*e1(1,t)+.5*e2(1,t)+.5*e3(1,t))*dt;% no Ms(1,t-1)
since clean water; -h(1,t)
    Mg(1,t)=-.5*e1(1,t)*dt+Mg(1,t-1);  %frac1*.5*h(1,t)*dt
    Md(1,t)=-.5*e2(1,t)*dt+Md(1,t-1);  %frac2*.5*h(1,t)*dt
    Mdd(1,t)=-.5*e3(1,t)*dt+Mdd(1,t-1); %frac3*.5*h(1,t)*dt

    end %for

    %------for x>1 for all t>1---------------------------------------
-


    for t=2:(DT/dt+1)

        e1old=e1(1,t);
        e2old=e2(1,t);
        e3old=e3(1,t);

        for x=2:TotalCells

            h(x,t)=vset*Ms(x,t-1)/D(x);
            if (h(x,t)*dt)>Ms(x,t-1)
                h(x,t)=Ms(x,t-1)/dt;
            end % if/else
```

```
            Mg1=Mg(x,t-1);
            Md1=Md(x,t-1);
            Mdd1=Mdd(x,t-1);

           if Mg1>(f_thresh*dx(x)*frac1)
            e1loc=a1*P*f_thresh*dx(x)*frac1;
           else
            e1loc=a1*P*Mg1;
           end

           if Md1>(dthresh*dx(x)*frac2)
            e2loc=a1*P*f_thresh*dx(x)*frac2; %should fthresh be here?
           elseif Md1>(f_thresh*dx(x)*frac2)
            e2loc=a2*P*f_thresh*dx(x)*frac2; % a1 or a2?
           else
            e2loc=a2*P*Md1;
           end



           if (Mdd1/dx(x))>(ddthresh*frac3)
            e3loc=a2*P*f_thresh*frac3*dx(x);
           elseif (Mdd1/dx(x))>(f_thresh*frac3)
            e3loc=a3*P*f_thresh*frac3*dx(x); % a2 or a3
           else
            e3loc=a3*P*Mdd1;
           end %if/else



            if (e1loc*dt)>Mg1
                e1loc=Mg1/dt;
            end % if/else

            if (e2loc*dt)>Md1
                e2loc=Md1/dt;
            end % if/else

            if (e3loc*dt)>Mdd1
                e3loc=Mdd1/dt;
            end % if/else

            Ms(x,t)=(.5*e1loc+.5*e1old)*dt+(.5*e2loc+.5*e2old)*dt+...
                (.5*e3loc+.5*e3old)*dt-(.5*h(x,t)+.5*h(x-
1,t))*dt+Ms(x-1,t-1);
            Mg(x,t)=-(.5*e1loc+.5*e1old)*dt+frac1*(.5*h(x,t)+.5*h(x-
1,t))...
                *dt+Mg(x,t-1); % should this be Mg(x-1,t-1)?
            Md(x,t)=-(.5*e2loc+.5*e2old)*dt+frac2*(.5*h(x,t)+.5*h(x-
1,t))...
                *dt+Md(x,t-1);
            Mdd(x,t)=-(.5*e3loc+.5*e3old)*dt+frac3*(.5*h(x,t)...
                +.5*h(x-1,t))*dt+Mdd(x,t-1);

            e1old=e1loc;
```

```
            e2old=e2loc;
            e3old=e3loc;

        end % x for


        MLoss(1)=0;
        MLoss(t)=Ms(TotalCells,t-1)+MLoss(t-1);
                  %MLoss - think of as if calculating
Ms(TotalCells+1,t)

    end % t for

    QMinP(i)=MLoss((DT/dt)+1)*(1/15); % calcs. cumul loss during int
per sec
    Time(i)=i*DT*60;  % in min.

% Total Mass
%Sum=sum(Ms(:,DT/dt+1))
Total=sum(QMinP)*15+sum(Ms(:,DT/dt+1))+sum(Mg(:,DT/dt+1))+...
    sum(Md(:,DT/dt+1))+sum(Mdd(:,DT/dt+1))
    Total=1;
%------End Interval
InitMs=1/Total*Ms(:,DT/dt+1);
InitMg=1/Total*Mg(:,DT/dt+1);
InitMd=1/Total*Md(:,DT/dt+1);
InitMdd=1/Total*Mdd(:,DT/dt+1);
%InitMgCum=MgCum(DT/dt);

end %for

%----Code to plot profiles instead of breakthrough ------------------
%length(1)=dx(1);
%for i=2:TotalCells
%    length(i)=dx(i)+length(i-1);
%end
%profile=Mg(:,1000)'./dx;
%plot(length,profile);

%xlabel('Position (cm.)');
%ylabel('Mass (g/cm)');
%axis([0 60 0 .6]);
%-----------------------------------------------------------------------
------

plot(Time,QMinP/3.7,'r-','LineWidth',2);  % divide QminP/.206?
%axis([0 T*60 0 .05]);
hold on
 %plot(UniformTime*60,UniLossRate/60,'s');
 plot(KTime*60,LossRateK2/60/3.7,'s','MarkerFaceColor','k');
  plot(KTime*60,LossRateK1/60/3.7,'s');
%plot(LongTime*60,(Long1adj),'s');
%plot(LongTime*60,(Long2adj),'s','MarkerFaceColor','k');
```

```
xlabel('Time (sec)');
ylabel('Mass Loss (g/sec)');
```

B.3- Chapter 2 Derivation of Selected Items

I. Analytical Solution to Two Bin MRMT Model

For a two bin MRMT model, Eqn's 1 and 2 in Chapter 2can be rewritten as:

$$\frac{\partial M_s}{\partial t} + u\frac{\partial M_s}{\partial x} = -kM_s + h_1 M_1 + h_2 M_2 \qquad \frac{\partial M_i}{\partial t} = kf_i M_s - h_i M_i \text{ for i=1,2}$$

(B1) & (B2)

where h_i is an ejection rate parameter and k is a capture rate parameter.
Using a Laplace transform, with an initial condition of $M_s(x,0) = \delta(x)$,
$\overline{M}_s(0) = \frac{H(x)}{u}$. a two bin model has the form:

$$\overline{M}_s(x) = \frac{H(x)}{u} e^{\frac{-kx}{u}} e^{\frac{-sx}{u}} \exp\left[\frac{kx}{u}\frac{f_1 h_1}{h_1 + s}\right] \exp\left[\frac{kx}{u}\frac{f_2 h_2}{h_2 + s}\right] \qquad \text{(B3)}$$

Using the convolution property in combination with the inverse transform (Oberhettinger & Badii, 1973, 5.66)

F(s): $e^{\frac{a}{s}} - 1$ f(t): $(\frac{a}{t})^{\frac{1}{2}} I_1[2(at)^{\frac{1}{2}}]$ (B4)

Eqn. B3 can be inverted to Eqn. 4 in Chapter 2.

II. Derivation of u_{eff} and D in terms of h_i and k

Taking Eqn.'s 1 and 2 in Chapter 2 and putting Eqn. 1 in terms of p only,

$$q_i = \frac{1}{h_i}(f_i k p - \frac{\partial q_i}{\partial t}) \qquad \text{(A5)}$$

$$\frac{\partial^n q_i}{\partial t^n} = \frac{1}{h_i}\left[f_i k \frac{\partial^n p}{\partial t^n} - \frac{\partial^{n+1} q_i}{\partial t^{n+1}}\right] \text{ for n=1,2,…} \qquad \text{(A6)}$$

Substituting into Eqn. 1 and cutting off terms greater than 2nd order:

$$\left(1 + \sum_{i=1}^{n} \frac{f_i k}{h_i}\right)\frac{\partial p}{\partial t} + u\frac{\partial p}{\partial x} = \left(\sum_{i=1}^{n} \frac{f_i k}{h_i^2}\right)\frac{\partial^2 p}{\partial t^2} \qquad \text{(A7)}$$

One can transform the *t* derivative into an *x* derivative using the relation:

$$\left(\frac{\partial}{\partial x}\right)^a = \left(\frac{-1}{u}\left(1+\sum_{i=1}^{n}\frac{f_i k}{h_i}\right)\frac{\partial}{\partial t}+\frac{1}{u}\left(\sum_{i=1}^{n}\frac{f_i k}{h_i^2}\right)\frac{\partial^2}{\partial t^2}\right)^a \qquad \text{(A8)}$$

Resulting, in the equation:

$$\frac{\partial p}{\partial t}+\frac{u}{1+k\left(\sum_{i=1}^{n}\frac{f_i}{h_i}\right)}\frac{\partial p}{\partial x}=\frac{u^2\left(\sum_{i=1}^{n}\frac{f_i k}{h_i^2}\right)}{\left\{1+k\left(\sum_{i=1}^{n}\frac{f_i}{h_i}\right)\right\}^3}\frac{\partial^2 p}{\partial x^2} \qquad \text{(A9)}$$

with the scalar of the first order *x* derivative analogous to effective velocity, u_{eff}, and the scalar of the second order *x* derivative analogous to a dispersion constant, *D*, similar to Lisle et al. (1998).